Andean Geology 52 (1): 63-85. January, 2025 doi: 10.5027/andgeoV52n1-3759

Phreatomagmatic mafic monogenetic volcanism related to salars: two case studies from the Puna plateau, Argentina

Daiana Orellana¹, *Pablo Grosse^{2,3}, Silvina R. Guzmán⁴, Walter A. Báez⁵, Facundo D. Apaza⁵

- Ganfeng Lithium Latinoamérica, Juramento 80, (4400) Salta, Argentina. daiananorellana 10@gmail.com
- ² Consejo Nacional de Investigaciones Científicas y Técnicas (CONICET), Godoy Cruz 2290, (C1425FQB) Buenos Aires, Argentina.
- ³ Fundación Miguel Lillo, Miguel Lillo 251, (4000) Tucumán, Argentina. pgrosse@lillo.org.ar
- ⁴ National Institute of Oceanography and Applied Geophysics (OGS), Borgo Grotta Gigante 42/c, (34010) Sgonico, Italy. silvinaraquelguzman@gmail.com
- ⁵ Instituto de Bio y Geociencias del NOA (IBIGEO), UNSa-CONICET, 9 de Julio 14, 4405, Rosario de Lerma, Salta, Argentina. geowbsalta@gmail.com, domingoapaza@gmail.com
- * Corresponding authors: pgrosse@lillo.org.ar

ABSTRACT. Mafic monogenetic volcanoes and salt pans or salars are ubiquitous in the Puna plateau of the Central Andes. In this contribution, we present the study of two Pleistocene mafic monogenetic centers, the Panqueque center emplaced on the western margin of the Salar de Arizaro and the Medialuna center emplaced within the same salar. Both centers had initial explosive phreatomagmatic activity that progressed to explosive magmatic (Strombolian) activity and ended with effusive activity. However, differences in magma flux, bedrock composition, and magma-water interaction resulted in deposits with different volumes and characteristics and, consequently, varied landforms. The magma batch that formed the Panqueque center (0.098 km³) passed through a heterogeneous bedrock marked by the transition between clastic and evaporitic deposits. Variable magma-water interaction generated two stages of phreatomagmatic activity, producing first a tuff ring or rings and then tuff cones, followed by Strombolian activity. Activity culminated with two phases of volumetrically dominant lava flows. In contrast, the much smaller Medialuna center (0.00016 km³) was formed by a magma batch that ascended through the mostly homogeneous halite-rich core of the salar. The magma interacted with water-saturated evaporitic sediments and fragmented close to the surface, generating a small asymmetric tuff ring. A minor final stage of magmatic activity consisted of ballistic fall activity and a lava cap at the conduit. The Panqueque center pyroclastic deposits do not show any specific feature that alludes to the salar environment, possibly because they formed at the salar margin where alluvial clastic sediments are abundant. Conversely, the Medialuna center deposits do have a few features, namely the lack of lithics, the possible total disintegration of the mechanically weak and friable evaporities into fine to very fine ash particles, and the presence of aggregates cemented by gypsum/salts that may be diagnostic of salar-related phreatomagmatic activity.

Keywords: Hydrovolcanism, Tuff ring, Tuff cone, Lava flow, Salt pan, Salar de Arizaro, Central Volcanic Zone of the Andes.

RESUMEN. Volcanismo freatomagmático monogenético máfico relacionado con salares: dos casos de estudio de la Puna, Argentina. Los volcanes monogenéticos máficos y los salares son abundantes en la Puna de los Andes Centrales. En esta contribución, se presenta el estudio de dos centros monogenéticos máficos pleistocenos, el centro Panqueque, ubicado en el margen oeste del salar de Arizaro, y el centro Medialuna, situado dentro del mismo salar. Ambos centros experimentaron actividad freatomagmática explosiva inicial que progresó a actividad magmática explosiva (estromboliana) y culminó con actividad efusiva. Sin embargo, diferencias en el flujo de magma, la composición del subsuelo y la interacción magma-agua dieron como resultado depósitos con diferentes volúmenes y características y,

en consecuencia, distintas geoformas. El magma que formó el centro Panqueque (0,098 km³) atravesó un subsuelo heterogéneo marcado por la transición entre depósitos clásticos y evaporíticos. Interacciones magma-agua variables generaron dos etapas de actividad freatomagmática, produciendo primero un anillo o anillos de toba y luego conos de toba, seguidos de actividad estromboliana y finalmente con dos fases de flujos de lava volumétricamente dominantes. Por el contrario, el centro Medialuna, mucho más pequeño en volumen (0,00016 km³), se formó a partir de magma que ascendió a través de un sector mayormente homogéneo y rico en halita dentro del salar. Este magma interactuó con sedimentos evaporíticos saturados en agua y se fragmentó cerca de la superficie, generando un pequeño anillo de toba asimétrico. Una etapa final de actividad magmática menor consistió en caída de fragmentos balísticos y un tapón de lava en el conducto. Los depósitos piroclásticos del centro Panqueque no muestran características específicas que aludan al ambiente del salar, posiblemente porque se formaron en el margen de este donde abundan los sedimentos clásticos aluviales. Por el contrario, los depósitos del centro Medialuna tienen algunas características, en particular la falta de líticos, la posible desintegración total de las evaporitas mecánicamente débiles y friables en partículas de ceniza fina a muy fina, y la presencia de agregados cementados por yeso/sales que pueden ser diagnósticas de actividad freatomagmática relacionada con salares.

Palabras clave: Hidrovolcanismo, Anillo de toba, Cono de toba, Flujo de lava, Salar de Arizaro, Zona Volcánica Central de los Andes,

1. Introduction

Monogenetic volcanism typically produces smallvolume and short-lived volcanoes that form during a single eruptive episode, but that can show a wide variety of eruption styles, stratigraphic architectures and geomorphologies (e.g., Németh and Kereszturi, 2015; Valentine and Connor, 2015). Explosive eruptions at monogenetic volcanoes can be purely magmatic, but also phreatomagmatic when the magmatic system interacts with surrounding sub-surface and/or surface water (e.g., Smith and Németh, 2017; Németh and Kósik, 2020). Magmatic explosive eruptions, without external water involvement, generally form scoria or spatter cones, whereas phreatomagmatic eruptions typically generate tuff cones, tuff rings, maars, and maar-diatremes (e.g., Vespermann and Schmincke, 2000; Kereszturi and Németh, 2012). Effusive activity forming lava flows are commonly associated with any of these landform types, but it can also form volcanoes on its own (e.g., Murcia and Németh, 2020).

The explosivity in monogenetic volcanic systems, and hence the resulting pyroclastic deposits and landforms, is controlled by several factors including the magma rheology and volatile content, the magma ascent rate or flux, the geometry and architecture of the system, the depth of fragmentation, the presence and abundance of external water, the effective magmawater ratio, and the degree of mixing between water and magma (*e.g.*, Vespermann and Schmincke, 2000; White and Ross, 2011; Valentine *et al.*, 2014; White and Valentine, 2016; Murcia and Németh, 2020).

The external water that may interact with magma generating phreatomagmatic eruptions can derive from surface water or groundwater (aquifers and water in sediments). In the specific case of aquifers, important factors that influence the degree and style of interaction with magma are their location and depth, recharge rate, lithology and permeability, and the abundance and physical properties of particles or fine sediments within them (e.g., White, 1996; Vespermann and Schmincke, 2000; Németh and Kósik, 2020; Planagumà et al., 2023). Salt pans or salars are particular groundwater sources as they typically consist of layers or mixtures of both clastic and evaporitic deposits, and hence have distinct hydrological and mechanical properties (e.g., Rosen, 1994; Giambastiani, 2020; Munk et al., 2021).

Monogenetic volcanism and salars converge in the Altiplano-Puna region of the Central Andes, which is part of the subduction-related Central Volcanic Zone of the Andes (e.g., Stern, 2004; Trumbull et al., 2006) (Fig. 1). The Altiplano (in Bolivia) and Puna (in Argentina) form a high-elevation and arid plateau containing abundant volcanic landforms and deposits, including hundreds of mafic monogenetic centers, and large endorheic basins that often host salars (e.g., Jordan et al., 1983; Alonso et al., 1991; Allmendinger et al., 1997).

Here, we describe mafic monogenetic volcanism, and in particular phreatomagmatism, related to a salar in the Puna plateau of northwestern Argentina. We characterize and reconstruct the eruptive histories of two such centers (here named Panqueque and Medialuna) emplaced at the margin of (Panqueque) and within (Medialuna) the Salar de Arizaro.

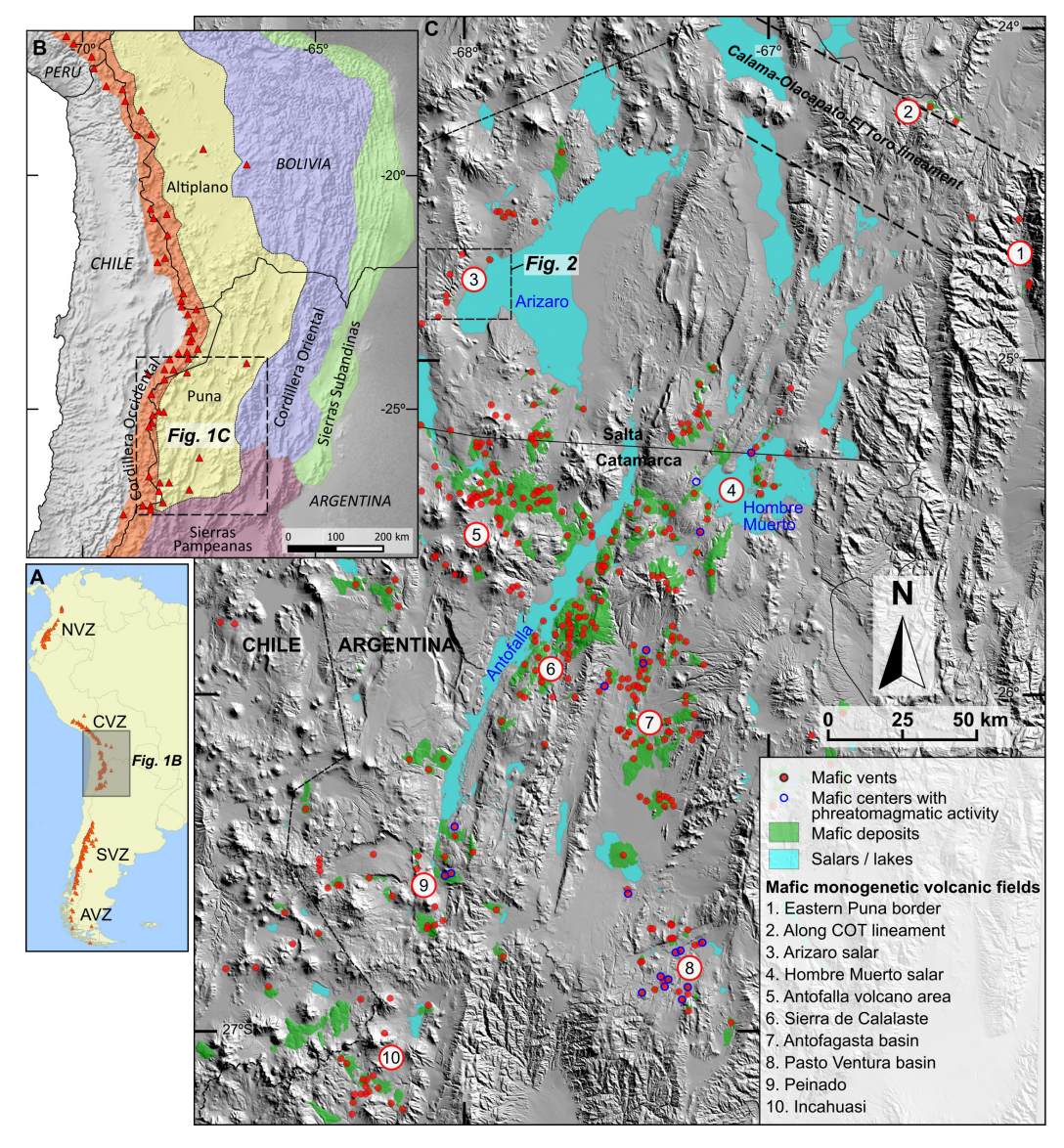


FIG. 1. A. Map of South America showing active/potentially active volcanoes (orange triangles) according to Siebert *et al.* (2010), and the volcanic zones of the Andes (NVZ: Northern Volcanic Zone; CVZ: Central Volcanic Zone; SVZ: Southern Volcanic Zone; AVZ: Austral Volcanic Zone). B. Location of the southern Puna within the CVZ, modified from Trumbull *et al.* (2006); red triangles are active/potentially active volcanoes. C. Spatial distribution of mafic monogenetic volcanism in the southern Puna, modified from Grosse *et al.* (2020); location of mafic centers with phreatomagmatic activity taken from Filipovich *et al.* (2019). The rectangle on the western margin of the Salar de Arizaro indicates location of figure 2. Background image is shaded relief map derived from a SRTM digital elevation model.

2. Geological setting

The Puna region of northwestern Argentina is a high-altitude plateau with crustal thickness up to ~75 km (Heit *et al.*, 2014; Beck *et al.*, 2015), crossed by longitudinal and transverse ranges that delimit extensive Tertiary and Quaternary valleys

that contain salars (Turner and Méndez, 1979; Jordan *et al.*, 1983; Salfity *et al.*, 2005). It hosts abundant volcanism from the Late Oligocene-Early Miocene until Present (*e.g.*, Petrinovic *et al.*, 2017). In particular, the Puna hosts profuse mafic monogenetic volcanism, mainly in its southern region (*e.g.*, Maro *et al.*, 2017).

2.1. Mafic monogenetic volcanism in the southern Puna

Mafic monogenetic volcanism in the southern Puna is represented by ~250 centers including scoria cones, tuff cones, tuff rings, maars, lava flows, and lava domes (Maro *et al.*, 2017; Haag *et al.*, 2019). These centers are spatially distributed in approximately ten main areas or fields (Fig. 1C) (*e.g.*, Grosse *et al.*, 2020). Their ages span from the Late Miocene (~7 Ma) until the Late Pleistocene, with peaks in activity at around 5-4 Ma and <1 Ma (Risse *et al.*, 2008; Schoenbohm and Carrapa, 2015).

Evidence of phreatomagmatism in the Puna region is scarce, possibly as a consequence of the long-lasting arid climate and the scarcity of water. However, mafic centers with features suggestive of phreatomagmatic activity are relatively abundant in the Pasto Ventura field (Fig. 1C), where Filipovich et al. (2019) documented three tuff rings, two maars, and four domes with initial phreatomagmatic phases. The greater abundance of phreatomagmatic activity in this field can be associated with its geographic position at the eastern Puna margin, where precipitation is higher than in the inner Puna (Filipovich et al., 2019). Other mafic centers with phreatomagmatic activity have been recognized in the Hombre Muerto, Antofagasta, and Peinado fields (Báez et al., 2017; Filipovich et al., 2019; Grosse et al., 2020) (Fig. 1C). All of the documented phreatomagmatic centers in the Puna seem to be associated with aquifers or lakes, but not directly with a salar. The only reported case, to our knowledge, of phreatomagmatic activity related to a salar is the Luna de Tierra tuff ring on the Carcote Salar, in the Cordillera Occidental, Chile, ~500 km north of our study area (Ureta et al., 2020).

2.2. The Salar de Arizaro volcanic field

The Salar de Arizaro monogenetic volcanic field extends along the southwestern margin of the Salar de Arizaro (Figs. 1 and 2). It consists of several mafic centers dominated by scoria and lava flows of basaltic andesite composition (Viramonte *et al.*, 1984; Boltshauser, 2011). There are seven ⁴⁰Ar/³⁹Ar ages (six on whole-rock and one on groundmass) for the mafic centers of the Salar de Arizaro field (Fig. 2; Schoenbohm and Carrapa, 2015; Maisonnave, 2016; Maisonnave and Poma, 2016). Ages range from 3.4±0.1 to 2.1±0.3 Ma for the oldest Chuculaqui-

Samenta center (three available ages; Fig. 2), whereas the other centers are younger, with ages <0.3 Ma (four available ages; Fig. 2).

The Panqueque and Medialuna mafic centers, the focus of this study, are part of the Salar de Arizaro field (Fig. 2). They are characterized by porphyritic rocks of basaltic andesite composition with olivine phenocrysts and clinopyroxene and plagioclase microphenocrysts immersed in a glassy groundmass (Maisonnave, 2016). A lava from the Panqueque center was dated at 0.22±0.07 Ma by Schoenbohm and Carrapa (2015), whereas the Medialuna center lacks absolute ages. Their deposits and volcanic evolution have not been described in detail and the role of phreatomagmatism has not been addressed before.

2.3. Salars in the Puna region and the Salar de Arizaro

The Altiplano-Puna region is characterized by salt pans or salars hosted in closed basins bounded by volcanic chains and tectonic blocks (*e.g.*, Alonso *et al.*, 1991; Riller and Oncken, 2003). The salars contain large volumes of continental evaporites (halite, sulfates, borates, carbonates) accumulated mainly since ~15 Ma (Alonso *et al.*, 1991; Vandervoort *et al.*, 1995). They generally show evaporite-dominated cores and transitional or mixing zones around the salar margins, where evaporitic and clastic deposits are interbedded (*e.g.*, Alonso, 2017).

The Salar the Arizaro, at 3,475 m a.s.l., is one of the largest salars of the Central Andes and the largest of Argentina with an area of ~1,700 km² (Fig. 1C). The salar formed within the ~100-kmdiameter Arizaro Basin, which contains Miocene lacustrine, fluvial, eolian, and evaporitic strata (DeCelles et al., 2015). It is a mature salar, with a thick halite core (Alonso et al., 1991; Rosko, 20221). Sources of water are surface water coming into the basin from its margins and groundwater inflow via alluvial fans (Rosko, 2022). Sampling trenches and exploration wells indicate a depth to the water table of less than ~1 m (Rosko, 2022). A 470 m deep well drilled in a central location of the salar, approximately 17 km east of the Medialuna mafic center, obtained a profile of crystalline halite (from 0 to 304 m), crystalline halite with some interbedded sand (304 to 364 m), fine sand with volcaniclastics and interbedded with halite (364 to 408 m), and fine brown sand (408 to 470 m) (Rosko, 2022).

Rosko, M. 2022. Results of year 2021 exploration activities and preliminary lithium resource estimate Salar de Arizaro project Salta province, Argentina. Interim Technical Report (Unpublished).

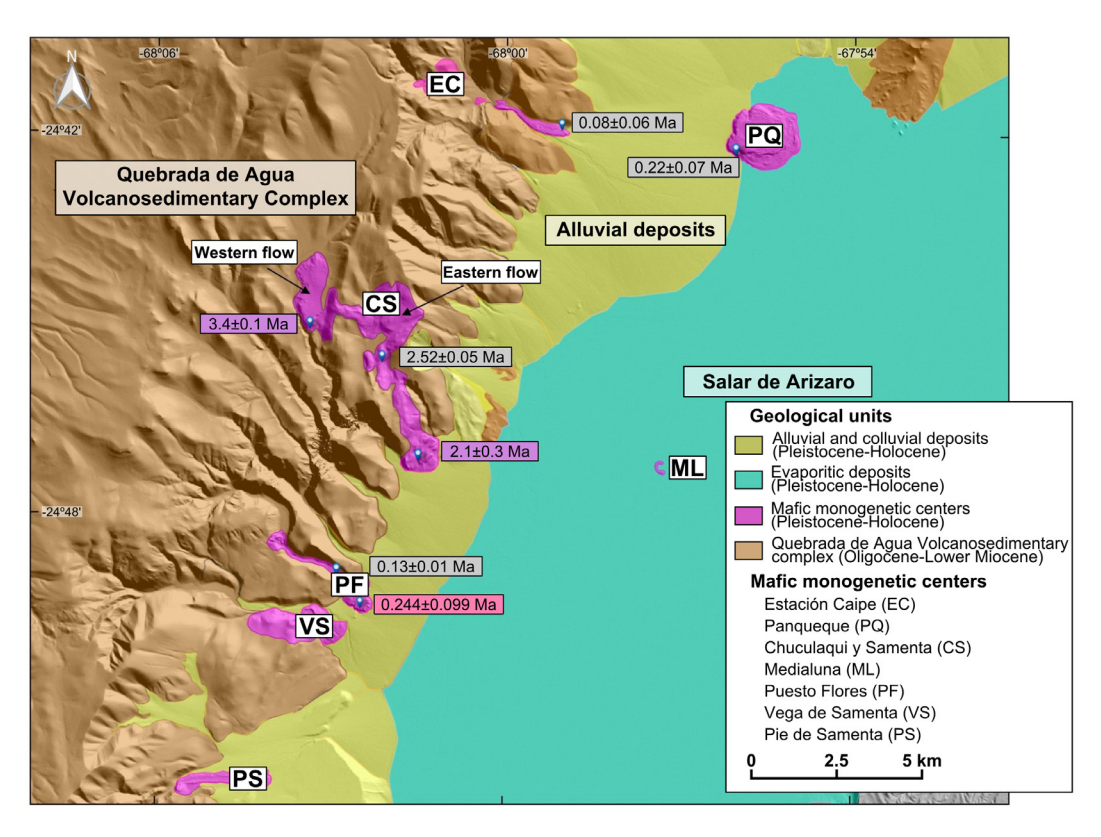


FIG. 2. Simplified geological map of the southwestern margin of the Salar de Arizaro (modified from Zappettini and Blasco, 2001) showing locations of mafic monogenetic centers and available ⁴⁰Ar/²⁹Ar ages (see Fig. 1C for map location). Four ages (light gray background) are from Schoenbohm and Carrapa (2015), two (purple background) are from Maisonnave and Poma (2016), and one (pink background) is from Maisonnave (2016). Background image is a TanDEM-X 12 m DEM-derived shaded relief.

3. Methods

Fieldwork consisted of mapping, description and sampling of the units that form the two studied centers. In the effusive units, lava flows were described and sampled. In the pyroclastic deposits, surface clasts and bombs were described, photographed and sampled, and three stratigraphic profiles from 50 to 60 cm depth (two in the Panqueque center and one in the Medialuna center) were excavated, described and sampled. In the Medialuna center, some bombs scattered on the salar around the center were identified and their major axes measured.

Cartography of the two centers was carried out with the QGIS software using a TanDEM-X 12 m spatial resolution digital elevation model (DEM) and optical satellite images of ~1 m resolution from Google Earth. The MORVOLC software (Grosse *et al.*, 2009, 2012) was used to estimate volumes, heights, areas, basal widths and slopes.

Nine samples of bombs, lava blocks and lava flows (six from the Panqueque center and three from Medialuna) were petrographically analyzed under a polarizing microscope. The size, shape and componentry of surface clasts from pyroclastic deposits was determined with a caliper and a hand lens. The abundance of the different surface clast types was estimated by point counting on field photographs.

Granulometric analysis was carried out on five samples of pyroclastic deposits from different horizons identified in the stratigraphic profiles; three samples correspond to the Panqueque center and two to the Medialuna center. Samples were sieved with a sieve stack with mesh sizes ranging from 32 to 1/16 mm (-5 ϕ to 4ϕ). Grain size was classified following White and Houghton (2006). Statistical analysis of the granolumetric results was carried out on Microsoft Excel; percentiles, mean, median, sorting, skewness, and kurtosis were calculated.

Size, roundness, vesicularity and componentry of the -2 to -1φ (4 to 2 mm), 0 to 1φ (1 to 0.5 mm), and 2 to 4φ (0.25 to 0.0625 mm) fractions of the five analyzed samples were estimated with a binocular lens. Roundness was defined following the traditional sedimentological classification proposed by Wadell (1933), which classifies fragments as very angular, angular, sub-angular, sub-rounded, rounded, and well rounded. Vesicularity was classified as low (<40 vol.%), moderate (40-60 vol.%), high (60-80 vol.%), and very high (>80 vol.%). For the componentry analysis, juvenile clasts, accidental lithic clasts, crystals and aggregates were recognized. Juvenile clasts were recognized as clasts of lava or scoria of mafic composition. Accidental lithic clasts were sub-divided into sedimentary (fragments of sedimentary rocks), metamorphic (phyllites), plutonic (fragments of granite, diorite or syenite rocks), and volcanic (fragments of andesite, dacite or rhyolite rocks). Volcanic lithic clasts and juvenile clasts were differentiated based on their contrasting compositions (juveniles more mafic, volcanic lithics more felsic). The abundance of each component was estimated by particle counting (200-300 particles per size fraction).

Morphological analysis of the pyroclastic material was carried out with a scanning electron microscope (SEM) at the Centro Integral de Microscopía Electrónica (Consejo Nacional de Investigaciones Científicas y Técnicas-Universidad Nacional de Tucumán). The 2 to 4ϕ (0.25 to 0.0625 mm) fractions, corresponding to fine and very fine ash, of each of the five samples were analyzed. Two parts from each fraction were analyzed, one cleaned (with distilled water) and one not.

4. Results

4.1. Panqueque mafic center

4.1.1. Stratigraphic units, morphology and morphometry

The Panqueque mafic center is located on the western margin of the Salar de Arizaro. Most of the center is emplaced on top of the salar, while the western part lays on top of an alluvial fan (Figs. 2 and 3). The center has a circular to sub-circular geometry, with a basal width of 1.9 to 2.2 km, covering an area of ~3.0 km² (Fig. 3). It has a flat morphology, with a height of ~60 m and a preserved volume of 9.8·10⁷ m³ (*i.e.*, 0.098 km³).

The Panqueque center is formed by a lower explosive unit and an upper effusive unit (Figs. 3 and 4A). The explosive unit consists of pyroclastic deposits that stand on top of the salar and crop out as a band or belt around the eastern part of the center (Fig. 3). The effusive unit consists of lava flows that radiate from a central emission point, located above the salar margin, and cover the explosive deposits and alluvial deposits to the west (Fig. 3).

4.1.2. Explosive unit: sub-units, componentry, and granulometry

The explosive unit has an exposed area of \sim 0.7 km² and an estimated volume of $8.8 \cdot 10^6$ m³ (*i.e.*, 0.0088 km³). These are minimum values as the lava flows of the upper effusive unit partially cover this unit. Two sub-units are identified, a main lower sub-unit, that spans most of the unit, and a minor upper sub-unit that consists of small low-sloping cone-shaped landforms located on top of the lower sub-unit (Figs. 3 and 4B).

The lower sub-unit crops out as a horseshoe-shaped strip with a width that varies between 40 and 370 m and a height or thickness of up to 30 m. It has a low topographic profile, with outer slopes <13° (mean of 7°) (Fig. 4A, B). The surface of the lower sub-unit is covered by lapilli- to block-sized juvenile fragments (95%) and lapilli-sized accidental fragments (5%). The juvenile fragments are mostly massive, with low vesicularity. Accidental fragments are sedimentary (chert), plutonic (syenites), volcanic (rhyolites), and metamorphic (phyllites).

The lower sub-unit excavated profile (50 cm) consists of an ochre-colored, palagonitized, massive, moderately consolidated, matrix-supported lapilli and ash facies (Facies 1) (Fig. 5A). It is formed by juvenile and accidental clasts of up to 5 cm in a fine ash matrix.

Three small, low-sloping cone-shaped landforms emplaced on top of the lower sub-unit are grouped as the upper sub-unit (Fig. 3). One of these landforms, located in the southern part of the center and here named Cone 1, was studied in the field (Figs. 3, 4B-C). The other two landforms, named Cone 2 and Cone 3, were only identified with satellite images (Fig. 3). Cone 1 is partially covered by a lava flow from the effusive unit (Fig. 4B, C), has a base of ~200 m, a height of ~30 m and a crater width of ~60 m. Its external flank has slopes of up to 15° (mean of 9°). Cone 1 is covered by mid to large bombs and lapilli-

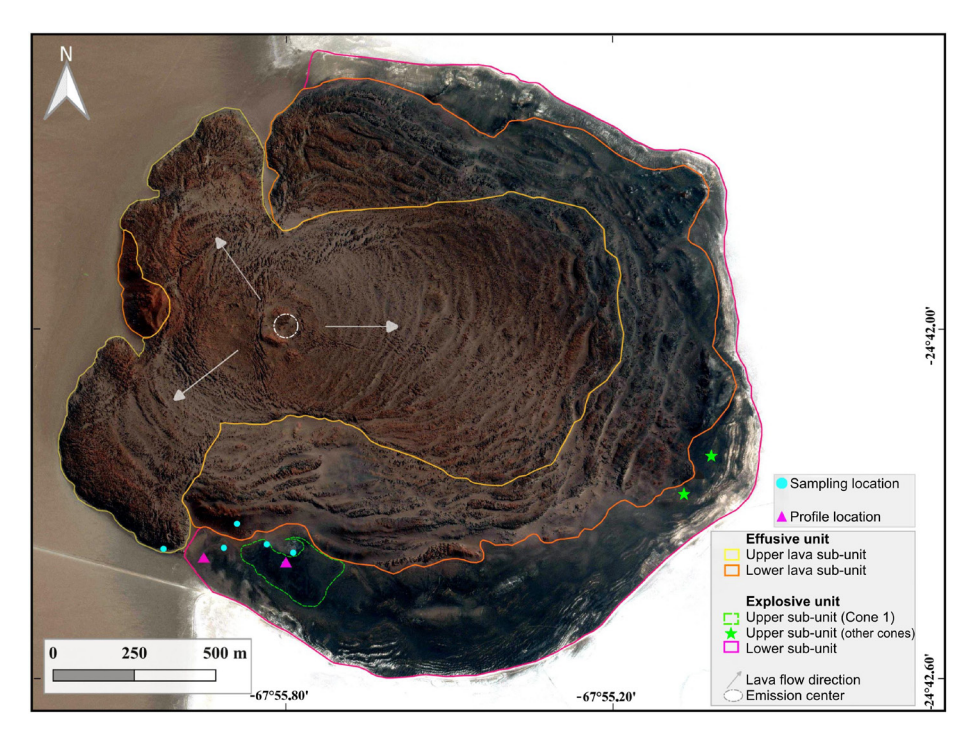


FIG. 3. Satellite image (from Google Earth) of the Panqueque mafic center with delineation of the identified units and sub-units; profile and sample locations are also shown.

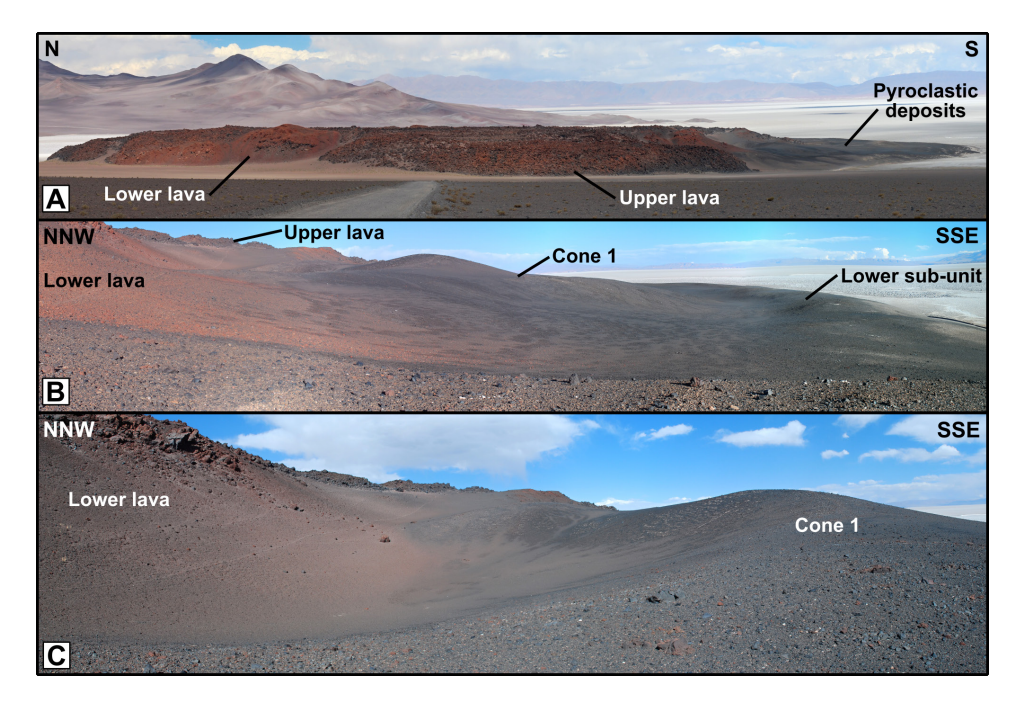


FIG. 4. A. Panoramic view of the Panqueque mafic center from the west, showing lava flows of the effusive unit covering pyroclastic deposits of the explosive unit. B. View of the SSW part of the Panqueque center, showing lava flows from the effusive unit and pyroclastic deposits from the lower and upper (Cone 1) sub-units of the explosive unit. C. Close-up of Cone 1; the northwest flank of the cone is covered by a lava flow from the effusive unit.

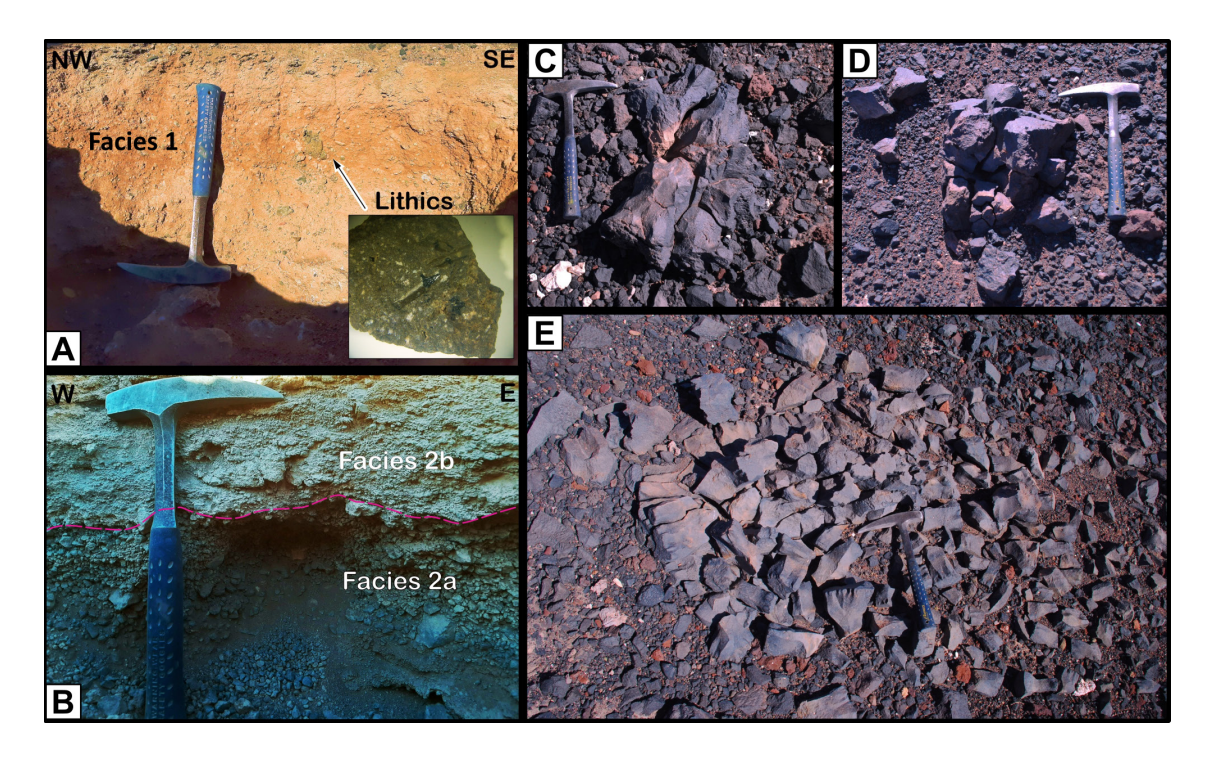


FIG. 5. Panqueque center, explosive unit. **A.** Profile of the matrix-supported lapilli and ash facies (Facies 1) of the lower sub-unit of the explosive unit. **B.** Profile of Cone 1 of the upper sub-unit, showing a lower clast-supported lapilli facies (Facies 2a) and an upper massive lapilli-and-ash facies (Facies 2b). **C-E.** Mid- to large-sized bombs on the surface of Cone 1; (**C**) bomb with prismatic jointing; (**D**) fractured bomb; (**E**) strongly fractured bomb with prismatic jointing.

to block-sized juvenile and accidental fragments. The juvenile fragments (85 vol.%) are mostly massive, with low to moderate vesicularity. The accidental fragments (15 vol.%) are plutonic (syenites), volcanic (porphyritic andesites and rhyolites), metamorphic (phyllites), and sedimentary (banded and fibrous chert-type travertines and cemented conglomerates), with sub-rounded to angular shapes. The bombs have sizes mostly between 0.5 and 2 m, some have rounded outlines and are usually fractured or show prismatic jointing (Fig. 5C-E). Under the microscope, the bombs have inequigranular porphyritic textures with olivine >> orthopyroxene phenocrysts (5-10 vol.%) and quartz > feldspar xenocrysts (< 1 vol.%), immersed in a microcrystalline light brown groundmass of plagioclase, olivine, pyroxene, and Fe-Ti oxide microlites and abundant vesicles.

The profile excavated in the Cone 1 deposit (42 cm) consists of two facies separated by an erosive contact, a lower clast-supported lapilli facies (Facies 2a), and an upper massive lapilli and ash facies (Facies 2b) (Fig. 5B). The gray-colored lower facies, >25 cm thick (unexposed base), is composed of fine-to-mid

lapilli with 1 to 3 cm sized juvenile black clasts. The beige-colored upper facies is 17 cm thick and is composed of mid-coarse ash to mid-lapilli with 1.5 to 3 cm sized juvenile black and accidental clasts.

Table 1 and figure 6 show granulometric distribution statistics and componentry of Facies 1 of the lower sub-unit and Facies 2a and 2b of the upper sub-unit. Facies 1 is poorly sorted and has a polymodal distribution, with a main mode in the fine ash fraction and a secondary mode in the medium lapilli fraction (Fig. 6A). Facies 2a is well sorted and has a unimodal distribution with a mode in the fine lapilli fraction and a very positive skewness (Fig. 6B). Facies 2b is also well sorted and has a symmetric unimodal distribution with a mode in the coarse ash fraction (Fig. 6C).

In Facies 1, the fine lapilli fraction is formed by 95 vol.% of angular to sub-angular accidental lithics (65 vol.% volcanic and 30 vol.% plutonic) and 5 vol.% of sub-angular juveniles (black and red, moderately to low vesicular fragments). The coarse ash fraction is formed by 59 vol.% of sub-rounded accidental lithics (43 vol.% volcanic and 16 vol.% plutonic),

FABLE 1. GRANULOMETRIC AND COMPONENTRY PARAMETERS OF THE PYROCLASTIC DEPOSITS OF THE EXPLOSIVE UNITS OF THE PANQUEQUE AND MEDIALUNA MAFIC CENTERS.

SSS Ku			Gra	Granulomet	ry (φ)							Componentry (%)	1try (%)					
ractes reducing skewitess ruitosis ne center -unit - Facies 2a -1,91 -1,77 1,53 0,33 0,97 -unit - Facies 2b 0,96 0,98 1,93 0,01 0,74 -a center		Median	Mean	Ι.	Classical	77		Fine lapilli	apilli			Coarse ash	e ash		I	Fine-Very fine ash	fine ash	
Le centerunit - Facies 1 0,58 -0,10 2,76 -0,18 0,66unit - Facies 2a -1,91 -1,77 1,53 0,33 0,97unit - Facies 2b 0,96 0,98 1,93 0,01 0,74 La center		Median	Mean		Skewness	SISOLINA	Лu	Ľ	Cx	$\mathbf{A}\mathbf{g}$	Лu	Li	Cx	Ag	Ju	Li	Cx	$^{\mathrm{Ag}}$
-unit - Facies 1 0,58 -0,10 2,76 -0,18 0,66 -unit - Facies 2a -1,91 -1,77 1,53 0,33 0,97 -unit - Facies 2b 0,96 0,98 1,93 0,01 0,74 ia center	eque center																	
-unit - Facies 2a -1,91 -1,77 1,53 0,33 0,97 -unit - Facies 2b 0,96 0,98 1,93 0,01 0,74 a center	sub-unit - Facies 1	0,58	-0,10		-0,18	99,0	5	95	,	,	6	59	30	2	×	XXX	XX	
ra center - 1,94 0,96 0,98 1,93 0,01 0,74 0,74 0.74 0.74 0.74 0.74 0.74 0.74 0.74 0.	sub-unit - Facies 2a	-1,91		1,53	0,33	0,97	86	2	,	,	85	13	7	,	,	,	ı	
a center 1,94 1,18 2,11 -0,36 0,94	sub-unit - Facies 2b	96,0	86,0	1,93	0,01	0,74	81	9		13	50	15	5	30	×	XXX	XX	
in center 1,94 1,18 2,11 -0,36 0,94																		
1,94 1,18 2,11 -0,36 0,94	luna center																	
1,94 1,18 2,11 -0,36 0,94		,	,	,	,	,	,	,	,	,	,	,	,	,	,	,	,	
		1,94	1,18	2,11	-0,36	0,94	100	,	,	,	100	,	,	,	XXX	,	,	
	3с	1,21	0,47		-0,30	0,80	66	1			91	2	4	3	XX		XX	

scalculated as the inclusive graphic standard deviation; skewness is calculated as the inclusive graphic skewness.

Ju: juveniles; Li: lithics; Cx: crystals; Ag: aggregates.
X's in fine-very fine ash componentry are rough estimations (x: scarce; xx: intermediate; xxx: abundant).

30 vol.% of crystals of quartz, feldspar and amphibole, 9 vol.% of black sub-angular juvenile fragments, and 2 vol.% of aggregates of lithic and juvenile fragments cemented in a fine ash matrix. The fine to very fine ash fraction consists of abundant plutonic and volcanic accidental lithics, crystals (plagioclase, olivine, quartz, and amphibole), and scarce black, low vesicular juvenile fragments.

In Facies 2a, the fine lapilli fraction is formed by 98 vol.% of juveniles and 2 vol.% of plutonic and volcanic accidental lithics. The juvenile clasts are black, low vesicular angular to sub-angular fragments (90 vol.%) and black/red, moderately vesicular sub-angular to sub-rounded fragments (8 vol.%). The coarse ash fraction is formed by juvenile clasts (85 vol.%; mostly black, low vesicular angular to sub-angular fragments), plutonic, volcanic and sedimentary accidental lithics (13 vol.%), and quartz and feldspar crystals (2 vol.%). The fine to very fine ash fraction consists of juvenile clasts (mostly black, low vesicular angular to sub-angular fragments), plutonic and volcanic accidental lithics, and crystals (plagioclase and K-feldspar).

In Facies 2b, the fine lapilli fraction is formed by 81 vol.% of juvenile clasts (black, low vesicular angular to sub-angular fragments), 6 vol.% of plutonic and volcanic accidental lithics, and 13 vol.% of aggregates (juvenile clasts and accidental lithics adhered to beige-colored ash). The coarse ash fraction is formed by 50 vol.% of the same type of juveniles, 15 vol.% of plutonic and volcanic accidental lithics, 30 vol.% of aggregates, and 5 vol.% of quartz and feldspar crystals. The fine to very fine ash fraction is formed by abundant volcanic accidental lithics, crystals (plagioclase, K-feldspar, olivine, quartz, and amphibole), and scarce black, low vesicular juvenile fragments.

Figure 7 shows SEM images of the fine to very fine ash fractions. Clasts are mostly poorly vesiculated and have blocky morphologies. They generally show rugged and irregular surfaces, and sub-angular, dented or concave-convex edges. Some clasts have step-like surfaces and moss-like aggregates are also found. Clasts are often covered by smaller particles adhered to their surfaces.

4.1.3. Effusive unit: sub-units and componentry

Most of the Panqueque center consists of an effusive unit formed by lava flows that radiate from a central emission point (Fig. 3). Stratigraphic relations and degree of alteration allow distinguishing two

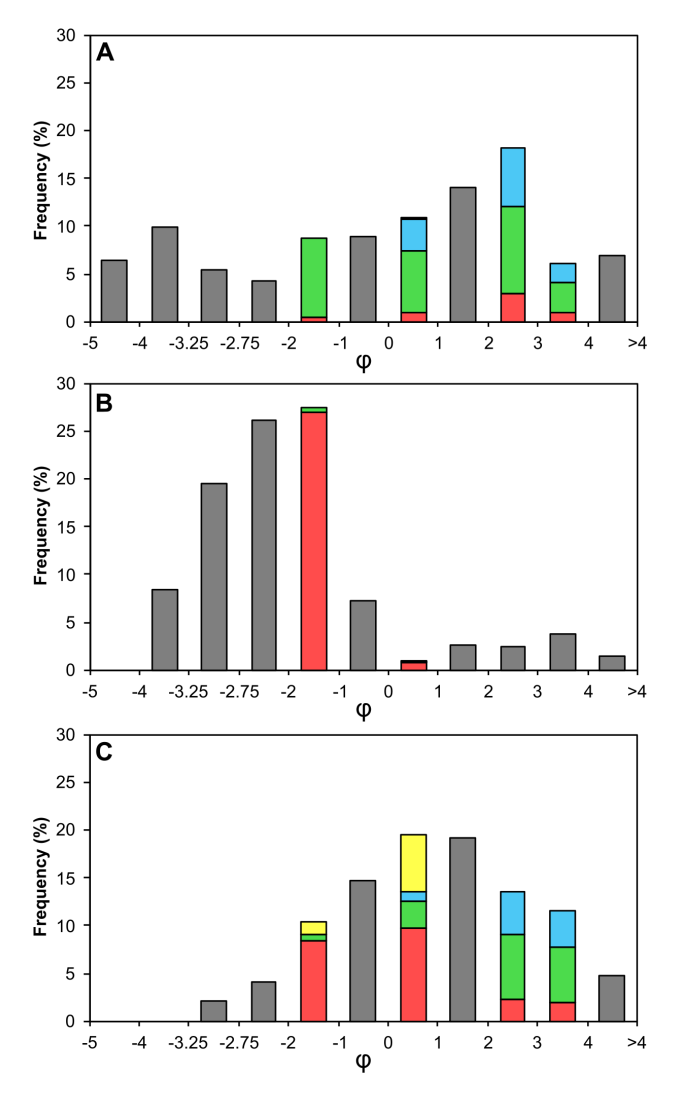


FIG. 6. Granulometric distribution histograms of Facies 1 (A) of the lower sub-unit, and Facies 2a (B) and 2b (C) of Cone 1 of the upper sub-unit (explosive unit, Panqueque center). Colors in φ fractions [-2 -1], [0 1], [2 3], and [3 4] indicate componentry; red: juveniles, green: lithics, blue: crystals, yellow: aggregates. Fractions without componentry analysis are displayed in gray.

sub-units, more degraded and reddish lower lavas, and less altered and grayish upper lavas (Figs. 3, 4, and 8).

The lower lavas flowed in all directions from the emission point, with a maximum travel distance of ~1.3 km eastwards (Fig. 3). The flows show thick and well-defined pressure ridges or ogives (Fig. 3) and have frontal thicknesses between ~10 and 40 m. The lavas are reddish and blocky, made up of massive, fractured and weathered blocks (Fig. 8A).

The upper lavas flowed 600 m towards the northwest, 750 m towards the southwest and 1 km towards the east (Fig. 3). The two western lobes

have 30 to 40 m thick fronts. The flow surfaces have pressure ridges and fractures sub-parallel to the flow directions (Fig. 3). The lavas are mostly blocky (Fig. 8B), although in some areas they are more rugged, showing characteristics of 'a'ā lava flows, with breccias and clinkers.

Both the lower and upper lavas have inequigranular porphyritic textures, with phenocrysts (5 to 10 vol.%) of olivine and occasionally orthopyroxene and plagioclase. Quartz xenocrysts (<1 vol.%) have reaction rims of pyroxene and glass. The groundmass consists of oriented plagioclase, olivine, pyroxene and Fe-Ti oxide microlites, and light brown glass.

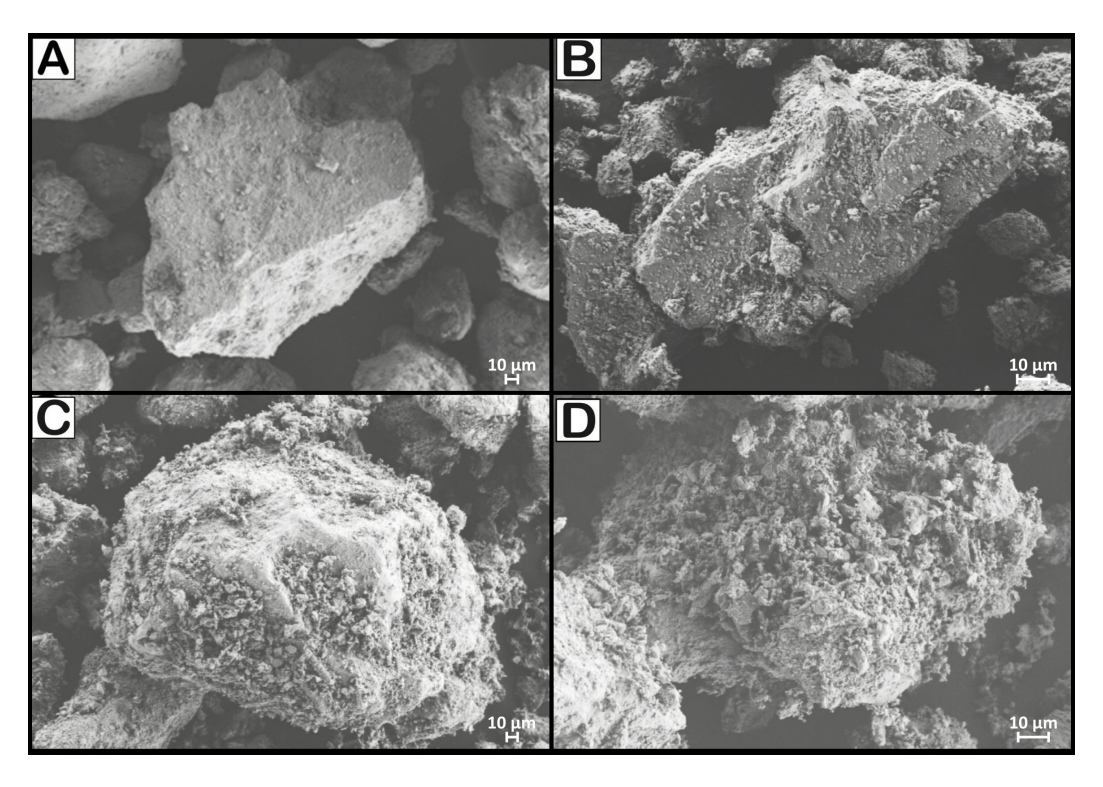


FIG. 7. Representative SEM images of the fine to very fine ash fractions (cleaned) of Facies 1 (A), 2a (B), and 2b (C-D) of the explosive unit of the Panqueque center. (A) Blocky clast with step-like surface and dented edges; (B-C) Blocky clasts with stepped surfaces covered by adhered particles; (D) Sub-rounded moss-like clast.

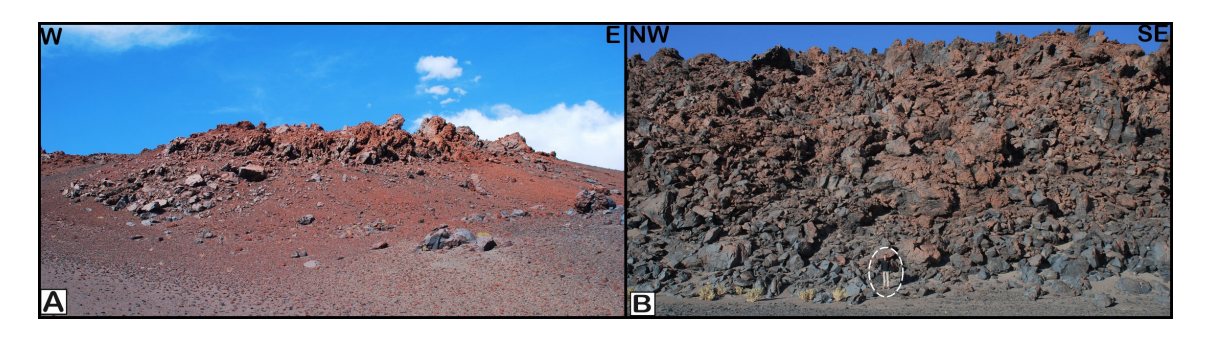


FIG. 8. Panqueque center, effusive unit. **A.** Reddish lava outcrop from the lower lava sub-unit. **B.** Gray, blocky lava outcrop from the upper lava sub-unit; note person for scale.

4.2. Medialuna mafic center

4.2.1. Stratigraphic units, morphology and morphometry

The Medialuna center is located within the Salar de Arizaro, 9 km south of the Panqueque center and 5 km from the western margin of the

salar (Fig. 2). It has a crescent moon or horseshoe plan shape, with an inner flank slopping eastward and an external flank sloping westward (Fig. 9). It has a north-south length of 390 m and a width that varies between 70 and 110 m (Fig. 9). Its height above the salar reaches a maximum of ~15 m at its southern tip (Fig. 10). It covers an

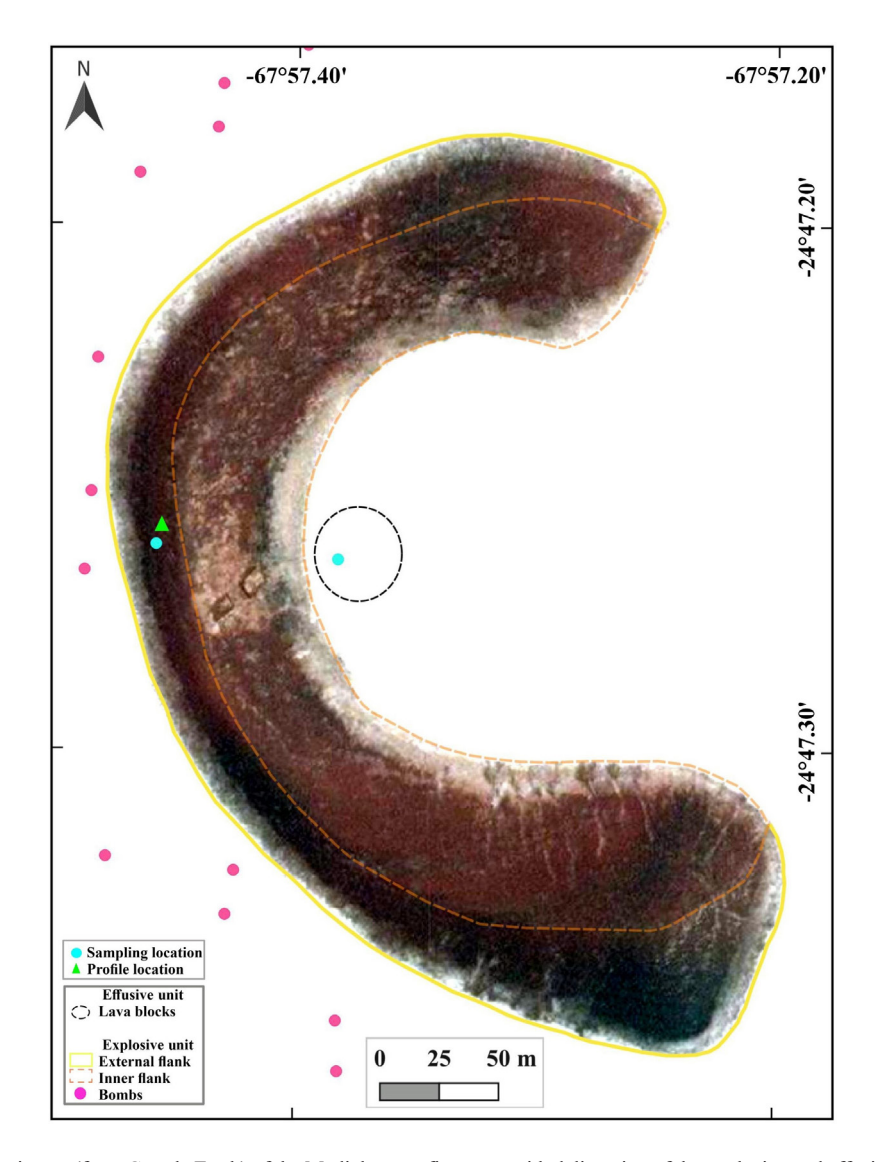


FIG. 9. Satellite image (from Google Earth) of the Medialuna mafic center with delineation of the explosive and effusive units; profile and sample locations are also shown.

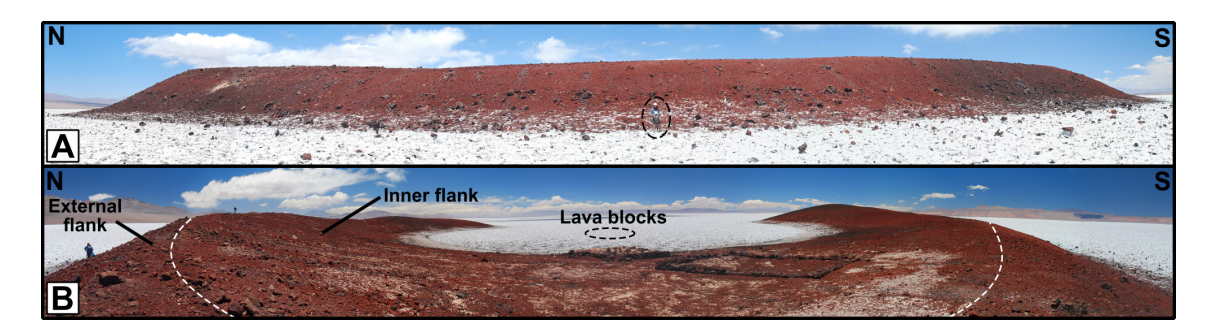


FIG. 10. Field photographs of the Medialuna mafic center. **A.** External flank slopping westward; note person for scale. **B.** Panoramic view of the explosive unit, showing inner and external flanks, and location of blocks of the effusive unit.

area of $0.04~\rm km^2$ and has an estimated preserved volume of $1.6\cdot 10^5~\rm m^3$ (i.e., $0.00016~\rm km^3$). The inner flank has mean slopes of 13° (measured in the field) and between 7-16° measured with the TanDEM-X DEM, whereas the external flank is steeper, with field-measured mean slopes of 25° and DEM-measured slopes of $9-19^\circ$.

The Medialuna center consists of a main explosive unit and a minor effusive unit (Fig. 9). The explosive unit is formed by pyroclastic deposits that make up the whole crescent-shaped landform, whereas the effusive unit consists of loose lava blocks east of the inner flank, scattered on top of the salar (Fig. 9).

4.2.2. Explosive unit: componentry and granulometry

The surface of the explosive unit is covered by small to large bombs and abundant lapilli-to-blocksized juvenile fragments. Small to medium bombs are also found west of the center, scattered on the salar (Fig. 9). The bombs on top of the deposit usually have aerodynamic and elongated shapes (Fig. 11A, B). Most bombs are reddish and can be massive, vesicular, or have vesiculated cores and massive margins. Dark gray, massive to vesicular bombs are less frequent. The larger bombs are usually strongly fractured (Fig. 11C) or show prismatic jointing, whereas some smaller bombs show breadcrust textures. The bombs scattered on the salar are found up to 100 m away from the external flank of the crescent-shaped landform (Fig. 9). They are massive or vesicular, black or reddish, with sizes between 15 and 60 cm, and have fusiform or elongated shapes and angular edges (Fig. 11D, E). On the surface of the deposit, 58 vol.% of juvenile fragments are lapilli-sized, sub-angular to angular, and 42 vol.% are fine blocksized, angular to very angular. The juvenile fragments are vesicular (53 vol.%) or massive (47 vol.%). No accidental fragments were found.

Under the microscope, massive bombs have inequigranular porphyritic textures with phenocrysts (10 vol.%) of olivine >> orthopyroxene and quartz xenocrysts (<1 vol.%), immersed in a groundmass of glass and plagioclase, pyroxene, and Fe-Ti oxide microlites. Vesicular bombs have phenocrysts (1-2 vol.%) of fractured and skeletal olivine immersed in a groundmass of dark brown glass and plagioclase, pyroxene and olivine microlites.

The excavated profile of the explosive unit (54 cm) has three facies (Fig. 11F), a lower, clast-

supported lapilli and bomb facies (Facies 3a), an intermediate, clast-supported lapilli with intercalations of laminated ash facies (Facies 3b), and an upper, matrix-supported lapilli and bomb facies (Facies 3c). Facies 3a has a minimum thickness of 12 cm (unexposed base) and consists of coarse lapilli to block-sized juvenile clasts (dense and vesiculated) and aggregates (juvenile clasts adhered to gypsum and ash) in a very coarse reddish ash matrix. Facies 3b is 14 cm thick and consists of clast-supported fineto-coarse lapilli, where the clasts are dense and vesiculated fragments. Part of this facies shows diffuse lamination. Facies 3c has a thickness of up to 28 cm. It contains lapilli to bomb-sized clasts of dense and vesiculated fragments, in a medium to coarse matrix.

Table 1 and figure 12 show granulometric distribution statistics and componentry of Facies 3b and 3c of the Medialuna center (Facies 3a was not analyzed). Facies 3b has poor sorting, very negative skewness, a main mode in the fine ash fraction and a minor secondary mode in the coarse ash fraction (Fig. 12A). Facies 3c is poorly sorted and has a polymodal distribution with negative skewness, with a main mode in the very fine ash fraction and a secondary mode in the coarse ash fraction (Fig. 12B).

In Facies 3b, all analyzed fractions are 100 vol.% composed of red or black, angular to sub-angular juvenile fragments. Clasts with moderate to high vesicularity predominate in the fine lapilli and coarse ash fractions, whereas both vesicular and massive clasts are found in the fine to very fine ash fraction.

In Facies 3c, the fine lapilli fraction is formed by 99 vol.% of juvenile clasts (81 vol.%: red or black, angular to sub-angular, moderate to highly vesicular; 18 vol.%: massive) and 1 vol.% of white, possibly sedimentary, accidental lithics. The coarse ash fraction is formed by 91 vol.% of juvenile clasts (63 vol.%: red or black, angular to sub-angular, moderate to highly vesicular; 28 vol.%: massive), 2 vol.% of plutonic and metamorphic accidental lithics, 4 vol.% of quartz crystals, and 3 vol.% of aggregates (juvenile clasts adhered to ash). The fine to very fine ash fraction contains juvenile clasts (red and black massive fragments) and crystals (quartz olivine and amphibole) in similar proportions.

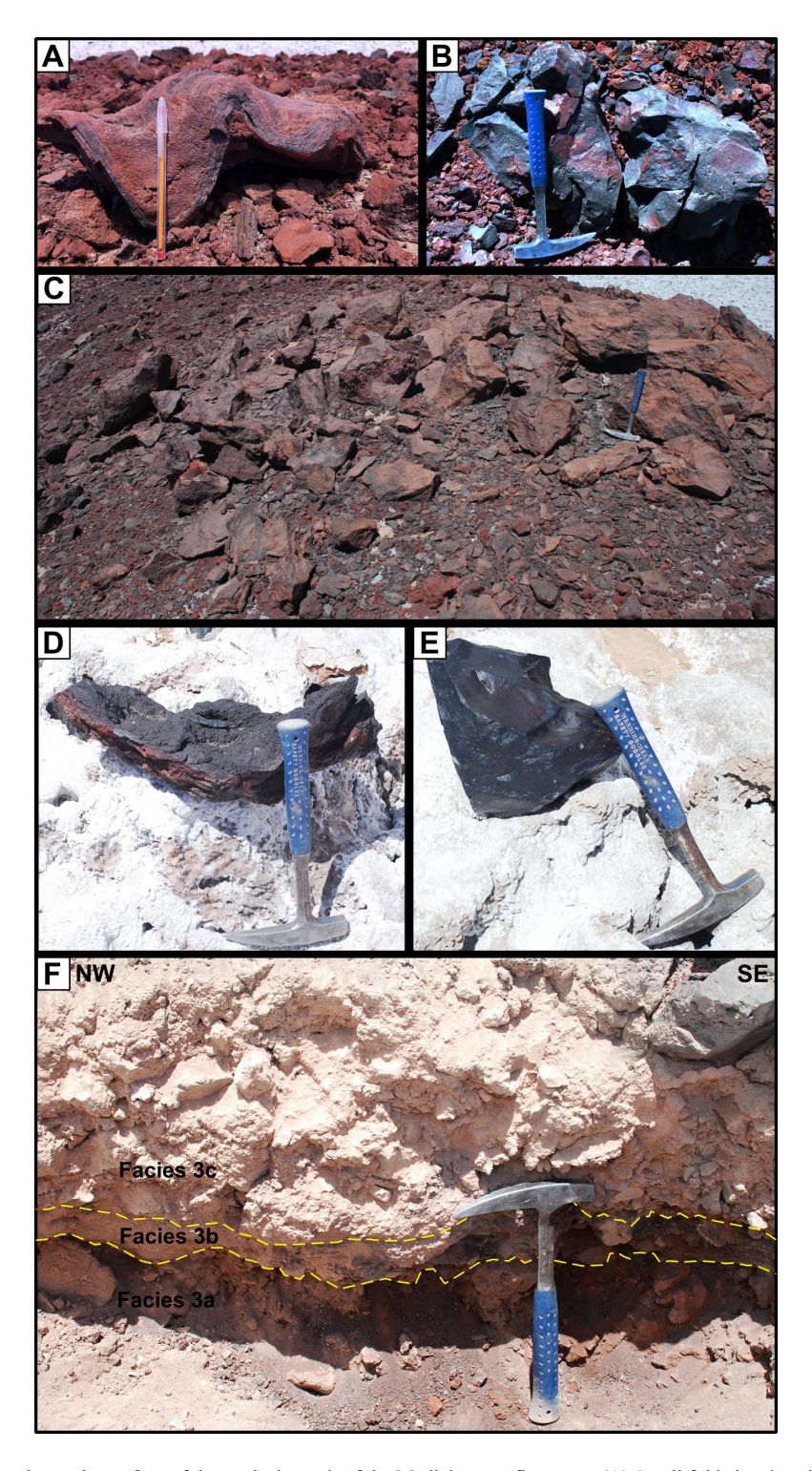


FIG. 11. A-C. Bombs on the surface of the explosive unit of the Medialuna mafic center: (A) Small folded and vesicular bomb with banding; (B) mid-sized massive, elongated bomb; (C) large, strongly fractured massive bomb. D-E. Bombs on the salar, west of the mafic center: (D) Fusiform vesicular bomb; (E) Massive angular bomb. F. Profile of the explosive unit showing three facies: lower, clast-supported lapilli and bomb facies (Facies 3a), intermediate, clast-supported lapilli facies (Facies 3b), and upper, matrix-supported lapilli and bomb facies (Facies 3c).

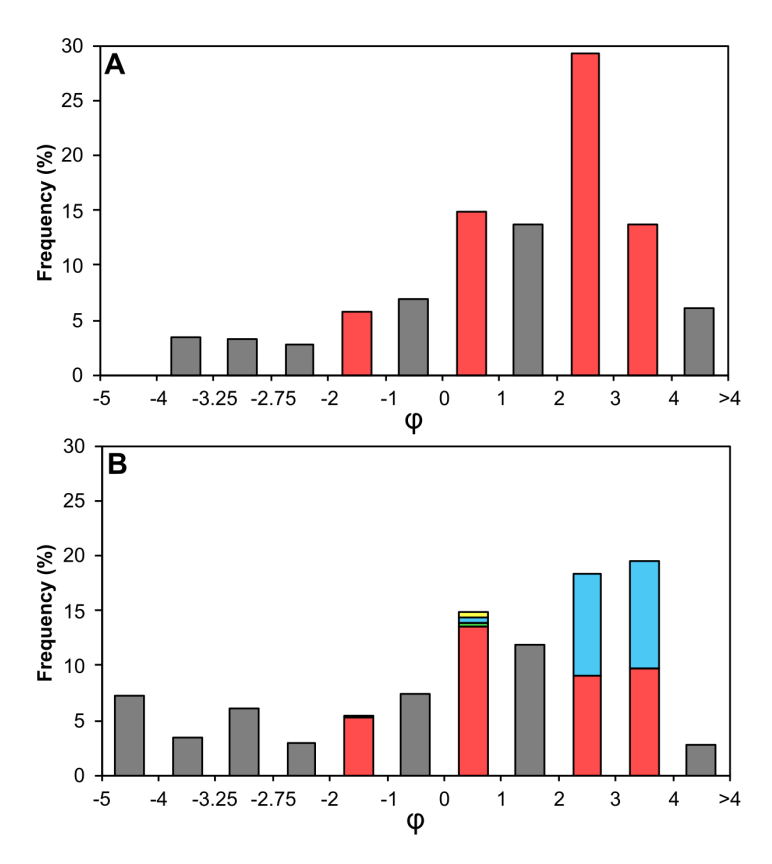


FIG. 12. Granulometric distribution histograms of Facies 3b (**A**) and Facies 3c (**B**) of the explosive unit of the Medialuna center. Colors in φ fractions [-2 -1], [0 1], [2 3], and [3 4] indicate componentry; red: juveniles, green: lithics, blue: crystals, yellow: aggregates. Fractions without componentry analysis are displayed in gray.

Figure 13 shows SEM images of the fine to very fine ash fraction. Clasts have blocky morphologies with rough and irregular or step-like surfaces. They are mostly massive, although some have moderate vesicularity. Finer particles are often adhered to the clast surfaces.

4.2.3. Effusive unit: componentry

The effusive unit is formed by lava blocks scattered on the salar about 10 to 20 m east of the inner margin of the crescent-shaped landform (Figs. 9 and 10B). This unit may be partially covered or buried by evaporite deposits, and we interpret it as a small lava flow or lava cap or plug at the emission point. The lava blocks are black, dense and massive, with angular edges and aphanitic textures. Under the microscope, they have an inequigranular porphyritic texture with phenocrysts (5 to 10 vol.%) of skeletal olivine and clinopyroxene and quartz xenocrysts

(<1 vol.%) with reaction rims of pyroxene, immersed in a hyalopilitic groundmass of glass and plagioclase, pyroxene and Fe-Ti oxide microlites.

5. Discussions

5.1. Features indicative of phreatomagmatism

The explosive units of the Panqueque and Medialuna centers have several features that suggest the interaction of magma with water in their formation. Although no feature is completely diagnostic by itself, the joint presence of several of them points towards phreatomagmatic activity (White and Valentine, 2016; Németh and Kósik, 2020, and references therein): (1) the morphologies and low slopes of the explosive unit landforms, which allow to classify them as tuff rings (the lower sub-unit of the Panqueque center and the explosive

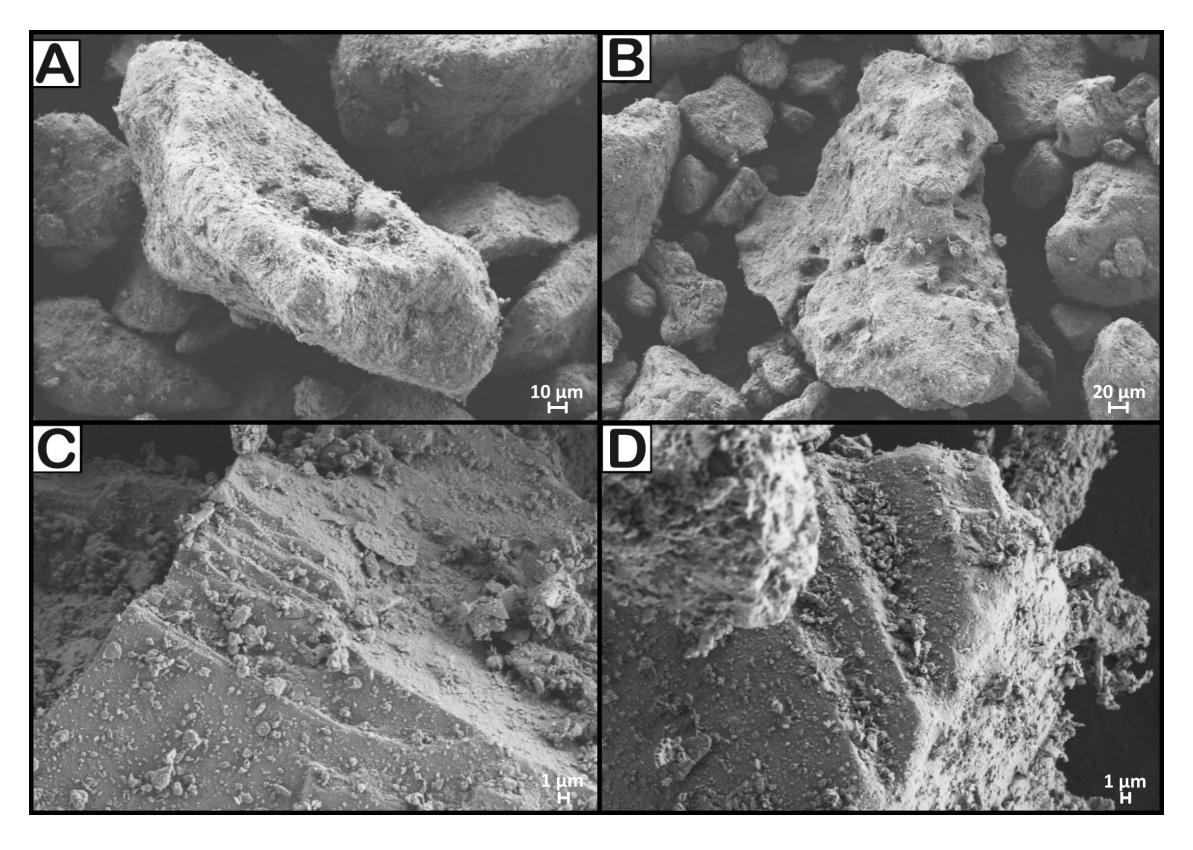


FIG. 13. Representative SEM images of the fine to very fine ash fractions (cleaned) of Facies 3b (A-B) and 3c (C-D) of the explosive unit of the Medialuna center. (A) Blocky clast with low vesicularity; (B) Sub-rounded clast with moderate vesicularity; (C-D) Massive clasts with step-like surfaces.

unit of the Medialuna center) and tuff cones (the upper sub-unit of the Panqueque center); (2) the abundance of lithic fragments in the Panqueque explosive unit (particularly in the lower sub-unit), although this is not the case for the Medialuna center (see below); (3) the mostly low vesicularity of clasts in the Panqueque explosive unit; (4) the presence of particle aggregates cemented by salts (especially in the Medialuna center); (5) the high proportion of fine to very fine ash particles in the lower sub-unit of the Panqueque center and in the Medialuna center; (6) palagonitization in the lower sub-unit of the Panqueque center; and (7) the typically blocky, massive morphologies, often with step-like surfaces and adhered particles, of the fine to very fine ash particles of all the analyzed facies. Overall, the sum of these features suggests that phreatomagmatic activity was an important process in the construction of both centers.

5.2. Transport and sedimentation mechanisms associated with the pyroclastic deposits

Panqueque's Facies 1 is a massive, poorly sorted, matrix-supported lapilli and ash facies with a high proportion of fine to very fine ash particles and abundant accidental lithic fragments. This facies is interpreted as the product of relatively energetic pyroclastic density currents (PDCs). Panqueque's Facies 2 has a lower, well-sorted, clast-supported lapilli facies (Facies 2a) and an upper, massive lapilli and ash facies (Facies 2b). Facies 2a is interpreted as a ballistic fall deposit generated by phreatomagmatic fragmentation, based on its clast-supported fabric, good sorting, and predominance of sub-angular, low vesicular clasts (e.g., Graettinger and Valentine, 2017; Filipovich et al., 2019; Valentine et al., 2022). Facies 2b may be associated with the deposition of PDCs, based on its massive character and high proportion of ash.

In the Medialuna center, the lower Facies 3a is clast-supported, unconsolidated, poorly sorted, and contains abundant lapilli to bomb-sized juvenile clasts. This facies is interpreted as the product of relatively low-energy ballistic curtains of dense tephra jets ejected laterally close to the emission source (e.g., Graettinger et al., 2015; Agustín-Flores et al., 2021). Facies 3b is lapilli-sized, clastsupported and contains diffuse laminations, whereas Facies 3c is matrix-supported, poorly sorted, with predominant lapilli-sized juveniles and subordinate bombs. Both facies are interpreted as the product of PDCs, Facies 3b more diluted and Facies 3c more concentrated, formed after the collapse of the dense tephra jets (e.g., Graettinger et al., 2015; Graettinger and Valentine, 2017).

5.3. Reconstruction of eruptive histories

Despite of the limited number and depth of the studied profiles, it is possible to propose reconstructions of the sequence of events that generated the Panqueque and Medialuna mafic centers.

5.3.1. Eruptive history of the Panqueque mafic center

The Panqueque volcano formed at 0.22±0.07 Ma (Schoenbohm and Carrapa, 2015) on the interdigitation between an alluvial fan and the Salar de Arizaro (Fig. 14A). The eruption started with the explosive interaction between an ascending feeder dyke of basaltic andesite composition and water-saturated unconsolidated sediments of the alluvial fan and/or the salar margin (Fig. 14B). Efficient fragmentation excavated the substrate and generated relatively high-energy PDCs (Fig. 14B), which resulted in pyroclastic deposits that accumulated around the eruptive vent(s), forming tuff ring(s) (the lower sub-unit) composed of abundant juvenile ash and accidental lithic fragments, and lower proportions of lapilli-sized juveniles (Fig. 14C).

During a second pulse, a smaller magma batch ascended to shallower levels and interacted less efficiently with the available water, generating lower-energy phreatomagmatic eruptions (Fig. 14D), which formed small tuff cones (the upper sub-unit) on top of the tuff ring(s) (Fig. 14E). During this stage, irregular magma-water interactions and/or variations in explosion depth produced different pulses, reflected in coarser and finer-grained facies (Facies 2a and 2b, respectively) (Fig. 14F).

The emplacement mechanisms of the tuff cones were ballistic fall of lapilli-sized fragments (Facies 2a) and PDCs that deposited massive ash layers (Facies 2b). The abundance of bombs in proximal areas indicates Strombolian-type ballistic emplacement during a final stage of cone construction (Fig. 14F), possibly associated with a depletion of the water supply due to an insufficient groundwater flow gradient (*e.g.*, Kshirsagar *et al.*, 2016).

After the explosive activity, a voluminous, purely magmatic effusive phase was established, possibly related to an increase in the magma flux. This effusive phase consisted of the emission of two lava flow pulses from a common source. In the first pulse, the lavas flowed in all directions, partially covering the explosive unit (Fig. 14G). In the second pulse, the lavas flowed towards the east, northwest and southwest, over the lavas of the first pulse and over the alluvial fan deposits (Fig. 14H).

5.3.2. Eruptive history of the Medialuna mafic center

The Medialuna center formed within the Salar de Arizaro, on a thick evaporitic sequence dominated by halite (Fig. 15A). An ascending feeder dyke reached a shallow level where it interacted with evaporitic layers saturated in water/brine and/or surface water, generating relatively low-energy phreatomagmatic eruptions whose products varied between laterally ejected ballistic curtains of dense tephra jets (Facies 3a) and PDCs (Facies 3b and 3c) (Fig. 15A). The strong asymmetry of the resulting crescentshaped tuff ring (Fig. 15B) may have been caused by an inclined feeder dyke (the dyke possibly changed its trajectory due to a decrease in host-rock stiffness at the base of, or within, the salar) that favored a directed eruption (e.g., Geshi and Neri, 2014; Bemis and Ferencz, 2017), i.e., an eruption with a lateral component towards the west. Preferential wind direction may have also played a role (e.g., Bertin, 2017), although it is unlikely that such an asymmetric landform could be due to horizontal winds only. The absence of lithics in the tuff ring deposits may be related to a shallow fragmentation level and to the evaporitic environment, in which the mechanically weak and friable evaporites disintegrated or were pulverized into fine to very fine ash particles. Also, some of the evaporites may have melted, given their low melting temperate (approximately 800 °C for halite, considerably lower for hydrated phases such as gypsum or carnallite; e.g., Warren, 2006;

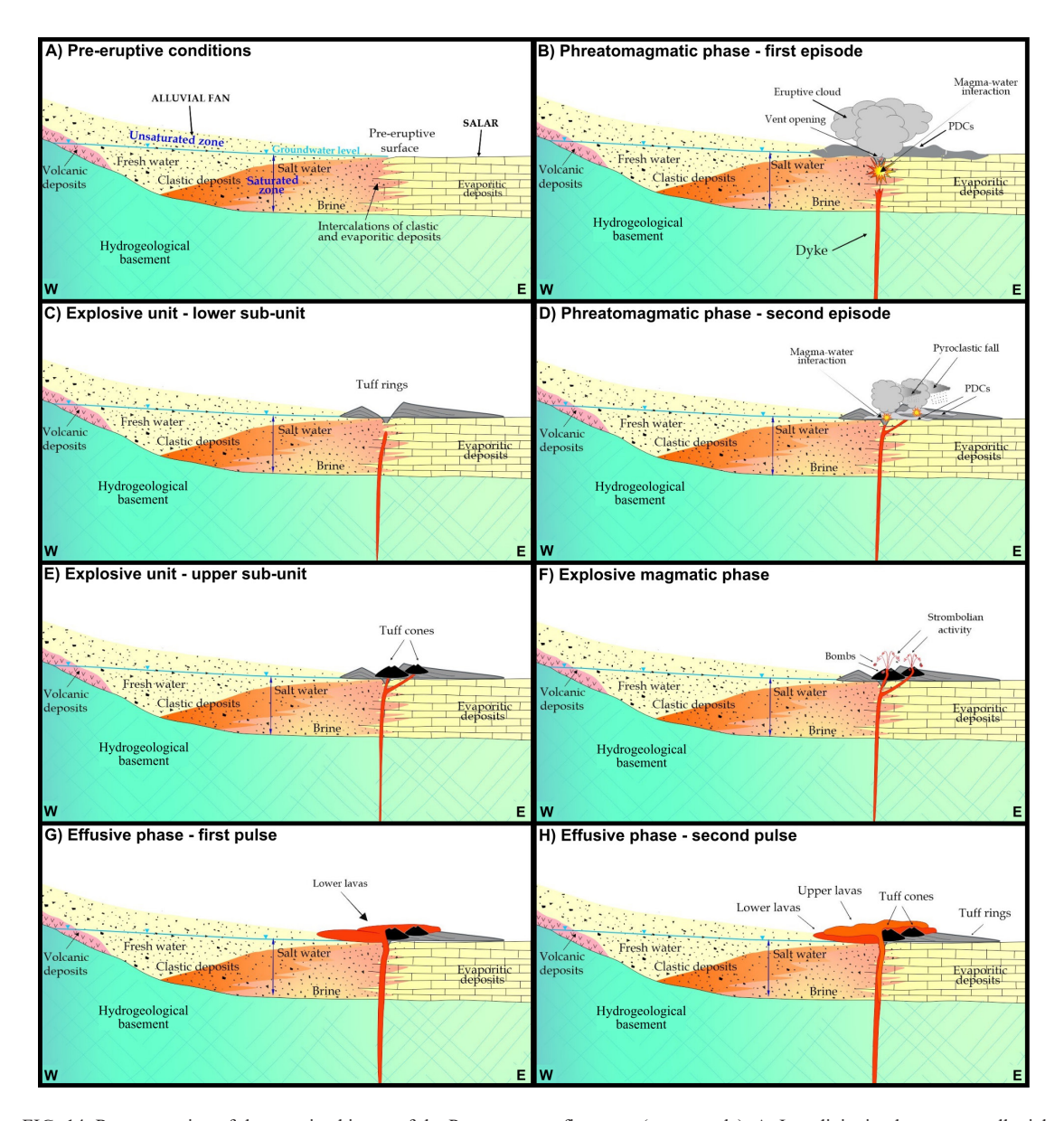


FIG. 14. Reconstruction of the eruptive history of the Panqueque mafic center (not to scale). A. Interdigitation between an alluvial fan and the Salar de Arizaro; conceptual model modified from García et al. (2016). B. Initial phreatomagmatic activity with vent opening/excavation and generation of PDCs. C. Formation of a complex tuff ring or rings. D. Second phreatomagmatic pulse generating pyroclastic fall and PDCs. E. Formation of tuff cones on top of the tuff ring(s). F. Strombolian activity with emplacement of bombs and pyroclastic fragments on the cones. G. First effusive pulse forming the lower lava flows. H. Second effusive pulse forming the upper lava flows.

Schofield *et al.*, 2014). Larger bombs were ejected at the end of the construction of the tuff ring, suggesting a shift toward Strombolian activity possibly marking a depletion in the water supply (Fig. 15C). The end of the eruption consisted in a minor effusive phase, with the emplacement of a small lava flow or cap in the vent area of the tuff ring (Fig. 15D).

5.4. Comparison between the two studied centers

The Panqueque and Medialuna centers share similarities but also show strong differences that can be related to different magma input/flux and their different positions with respect to the salar. Both centers show a similar sequence of initial

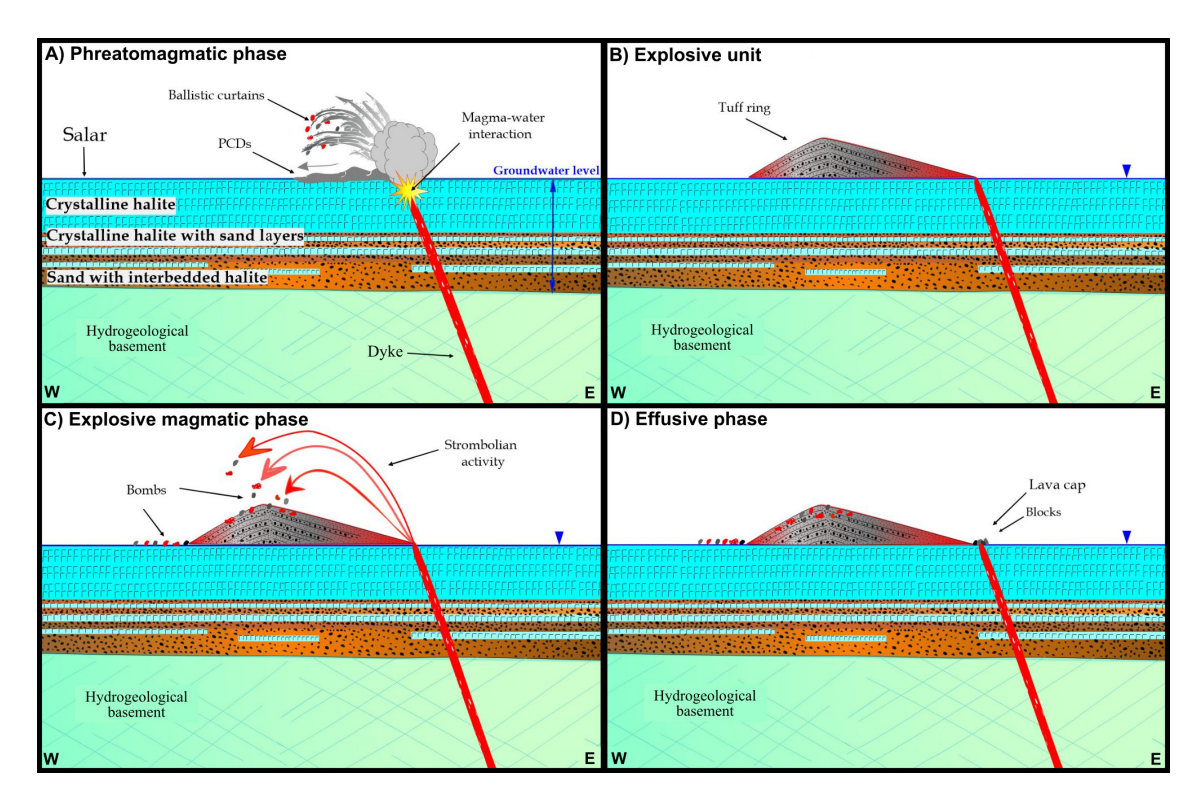


FIG. 15. Reconstruction of the eruptive history of the Medialuna mafic center (not to scale). The stratigraphic profile is inferred based on data from exploration drilling carried out in the Salar de Arizaro (Rosko, 2022). A. Phreatomagmatic activity caused by the interaction between an ascending magma dyke and evaporitic layers saturated in water/brine and/or surface water.

B. Formation of an asymmetric tuff ring west of the conduit. C. Emplacement of large bombs and pyroclasts (Strombolian activity). D. Emplacement of a small lava cap in the vent area of the tuff ring.

phreatomagmatic activity followed by a magmatic explosive phase (Strombolian) and culminating with effusive activity. This sequence has been documented at many mafic monogenetic centers worldwide (e.g., Kshirsagar et al., 2016; Pedrazzi et al., 2022). However, the volume and proportions of the different phases vary between the two centers. The overall volume of the Panqueque center is almost three orders of magnitude greater than the Medialuna center. Also, in the Panqueque center the effusive phase is volumetrically dominant, whereas in the Medialuna center the effusive phase is negligible. Magma input at Panqueque was much greater, possibly with a high enough flux to dry out the water supply and produce a significant effusive phase.

The location of the Panqueque center on the edge of the salar and on an alluvial fan suggests an interdigitation at depth between clastic and evaporitic sediments, where water may be distributed heterogeneously due to the alternation of sedimentary layers with different physical properties. On the other

hand, the location of the Medialuna center within the salar suggests a more homogeneous stratigraphic column of mostly evaporitic sediments with abundant and more uniformly distributed water. The greater abundance in water, coupled with a low magma flux, possibly led to lower fragmentation/explosivity and lower-energy eruptions at Medialuna.

The lower explosive sub-unit of the Panqueque center has a great abundance and variety of accidental lithic clasts, suggesting that the phreatomagmatic explosions excavated and incorporated host rock material, either directly from the alluvial fan and/or from greater depths. The upper explosive sub-unit contains less accidental lithics than the lower sub-unit, suggesting that the explosions were shallower and/or that the magma ascended through an established conduit. In strong contrast, the Medialuna center lacks accidental lithic clasts. It is made up of juvenile clasts and has a high proportion of fine particles (fine to very fine ash fraction); it also commonly has aggregates cemented by gypsum/salts. We suggest that in the

Medialuna center the magma-water interaction occurred exclusively within an evaporitic environment that lacked accidental lithic clasts (consistent with the top ~300 m thick halite layer documented by Rosko, 2022), producing the pulverization/disintegration of the mechanically weak and friable evaporite sediments, which comprise the fine to very fine ash fraction observed in the deposits. This may be akin to phreatomagmatic activity related to unconsolidated coastal plain sediments described by Agustín-Flores et al. (2014), where the accidental material was essentially found as an ash-sized matrix. Finally, the aggregates observed at Medialuna may be the result of precipitation of the disintegrated evaporites. All these features may be diagnostic of salar-hosted phreatomagmatism elsewhere.

6. Conclusions

The two studied centers are cases of mafic monogenetic volcanism that interacted with a salar, one at its margin (Panqueque center) and the other within it (Medialuna center). Both centers show a similar progression of explosive phreatomagmatic to explosive magmatic (Strombolian) to effusive activity, although the volumetric output of each phase and the resulting landforms varied in each center. In the Panqueque center, a relatively large magma input through the transitional zone between the salar and an alluvial fan, characterized by interdigitation of clastic and evaporitic deposits and variable water contents, generated two stages of phreatomagmatic activity, producing first a tuff ring or rings and then tuff cones that were capped by Strombolian activity. The final activity consisted of the effusion of volumetrically dominant lava flows, suggesting that magma input was large and/or fast enough to deplete the water supply. In contrast, the Medialuna center was formed by a much smaller magma batch that ascended through a mostly homogeneous water-saturated halite-rich core. The magma batch, although small, possibly ascended at a fast rate so as to reach the near-surface, where it interacted with the evaporitic sediments to produce phreatomagmatic activity and a small asymmetric tuff ring.

The pyroclastic deposits of the Panqueque center do not have any particular feature that points to the salar environment, possibly because they formed at the salar margin where clastic sediments are abundant. On the other hand, the Medialuna deposits do show a few features, namely the lack of lithics, the possible total disintegration of the mechanically weak and friable evaporites into fine to very fine ash particles, and the presence of aggregates cemented by gypsum/salts, that may be diagnostic of salar-related phreatomagmatic activity elsewhere.

Acknowledgements

This work stems from DO's undergraduate thesis at Universidad Nacional de Salta. It was funded by the Agencia Nacional de Promoción Científica y Tecnológica (Argentina) project PICT-2017-2798 and by Fundación Miguel Lillo (Tucumán, Argentina) project G-0033-1. The TanDEM-X digital elevation model was provided by the German Aerospace Center (DLR) through proposal DEM GEOL1342. Thin sections were done at the Laboratorio de Mineralogía y Petrografía of the Universidad Nacional de Salta. Granulometric analysis was carried out at the Instituto de Paleontología y Sedimentología of the Fundación Miguel Lillo; we thank C. Muruaga, S. Avellaneda, D. Guevara (RIP) and E. Burgos for their help. S. Décima is thanked for assistance in the field. We thank the reviewers H. Murcia and G. Valentine, as well as editor D. Bertin, for their thorough and insightful comments.

References

Agustín-Flores, J.; Németh, K.; Cronin, S.J.; Lindsay, J.M.; Kereszturi, G.; Brand, B.D.; Smith, I.E. 2014. Phreatomagmatic eruptions through unconsolidated coastal plain sequences, Maungataketake, Auckland volcanic field (New Zealand). Journal of Volcanology and Geothermal Research 276: 46-63. https://doi.org/10.1016/j.jvolgeores.2014.02.021

Agustín-Flores, J.; Siebe, S.; Ferrés, D.; Sieron, K.; González-Zuccolotto, K. 2021. Monogenetic volcanoes with initial phreatomagmatic phases in the Ceboruco graben, western Mexico: The cases of Potrerillo I, Potrerillo II, and San Juanito. Journal of Volcanology and Geothermal Research 412: p. 107184. https://doi.org/10.1016/j.jvolgeores.2021.107184

Allmendiger, R.; Jordan, T.; Kay, S.M.; Isacks, B. 1997. The evolution of the Altiplano-Puna plateau of the Central Andes. Annual Review of Earth and Planetary Sciences 25: 139-174. https://doi.org/10.1146/annurev.earth.25.1.139

Alonso, R.N. 2017. Los salares de la Puna argentina y su recurso minero. *In* Ciencias de la Tierra y Recursos Naturales del NOA (Muruaga, C.M.; Grosse, P.; editors).

- *In* Congreso Geológico Argentino, No. 20, Relatorio: 1018-1038. San Miguel de Tucumán.
- Alonso, R.N.; Jordan, T.E.; Tabbutt, K.T.; Vandervoort, D.S. 1991. Giant evaporite belts of the Neogene Central Andes. Geology 19 (4): 401-404. https://doi.org/10.1130/0091-7613(1991)019%3C04 01:GEBOTN%3E2.3.CO;2
- Báez, W.; Carrasco Núñez, G.; Giordano, G.; Viramonte, J.G.; Chiodi, A. 2017. Polycyclic scoria cones of the Antofagasta de la Sierra basin, Southern Puna plateau, Argentina. *In* Monogenetic Volcanism (Németh, K.; Carrasco-Núñez, G.; Aranda-Gómez, J.J.; Smith, I.E.M.; editors). The Geological Society, Special Publication 446 (1): 311-336. London. https://doi.org/10.1144/SP446.3
- Beck, S.; Zandt, G.; Ward, K.; Scire, A. 2015. Multiple styles and scales of lithospheric foundering beneath the Puna Plateau, central Andes. *In* Geodynamics of a Cordilleran Orogenic System: The Central Andes of Argentina and Northern Chile (DeCelles, P.G.; Ducea, M.N.; Carrapa, B.; Kapp, P.A.; editors). Geological Society of America Memoirs 212: 43-60. https://doi.org/10.1130/2015.1212(03)
- Bemis, K.G.; Ferencz, M. 2017. Morphometric analysis of scoria cones: the potential for inferring process from shape. *In* Monogenetic Volcanism (Németh, K.; Carrasco-Núñez, G.; Aranda-Gómez, J.J.; Smith, I.E.M.; editors). Geological Society of London, Special Publications 446 (1): 61-100. https://doi.org/10.1144/SP446.9
- Bertin, D. 2017. 3-D ballistic transport of ellipsoidal volcanic projectiles considering horizontal wind field and variable shape-dependent drag coefficients. Journal of Geophysical Research, Solid Earth 122 (2): 1126-1151. https://doi.org/10.1002/2016JB013320
- Boltshauser, B. 2011. Ocurrencia y petrología de volcanes monogenéticos cuaternarios en el salar de Arizaro, Puna Austral. Trabajo de tesis (Inédito). Universidad Nacional de Córdoba: 104 p.
- DeCelles, P.G.; Carrapa, B.; Horton, B.K.; McNabb, J.; Gehrels, G.E.; Boyd, J. 2015. The Miocene Arizaro Basin, central Andean hinterland: Response to partial lithosphere removal? *In* Geodynamics of a Cordilleran Orogenic System: The Central Andes of Argentina and Northern Chile (DeCelles, P.G.; Ducea, M.N.; Carrapa, B.; Kapp, P.A.; editors). Geological Society of America Memoirs 212: 359-386. https://doi.org/10.1130/2015.1212(18)
- Filipovich, R.; Báez, W.; Bustos, E.; Villagrán, A.; Chiodi, A.; Viramonte, J.G. 2019. Estilos eruptivos asociados al volcanismo monogenético máfico

- de la región de Pasto Ventura, Puna Austral, Argentina. Andean Geology 46 (2): 300-335. http://dx.doi.org/10.5027/andgeov46n2-3091
- García, R.; Rocha Fasola, V.; Moya Ruiz, F. 2016.
 El agua subterránea en la Puna Salteña. Argentina.
 Recurso estratégico para el desarrollo de la región.
 In Congreso Argentino de Geología Económica,
 No. 11, Relatorio Asociación Argentina de Geólogos
 Economistas. Salta.
- Geshi, N.; Neri, M. 2014. Dynamic feeder dyke systems in basaltic volcanoes: the exceptional example of the 1809 Etna eruption (Italy). Frontiers in Earth Science 2: 13. https://doi.org/10.3389/feart.2014.00013
- Giambastiani, M. 2020. Geomechanical characterization of evaporitic rocks. *In* Soft rock mechanics and engineering (Kanji, M.A.; He, M.; Sousa, L.R.; editors). Springer, Cham: 129-161. Switzerland. https://doi.org/10.1007/978-3-030-29477-9_6
- Graettinger, A.H.; Valentine, G.A. 2017. Evidence for the relative depths and energies of phreatomagmatic explosions recorded in tephra rings. Bulletin of Volcanology 79: 88. https://doi.org/10.1007/s00445-017-1177-x
- Graettinger, A.H.; Valentine, G.A.; Sonder, I.; Ross, P.S.; White, J.D.L. 2015. Facies distribution of ejecta in analog tephra rings from experiments with single and multiple subsurface explosions. Bulletin of Volcanology 77 (8): 66. https://doi.org/10.1007/s00445-015-0951-x
- Grosse, P.; van Wyk de Vries, B.; Petrinovic, I.A.; Euillades, P.A.; Alvarado, G.E. 2009. Morphometry and evolution of arc volcanoes. Geology 37 (7): 651-654. https://doi.org/10.1130/G25734A.1
- Grosse, P.; van Wyk de Vries, B.; Euillades, P.A.; Kervyn, M.; Petrinovic, I.A. 2012. Systematic morphometric characterization of volcanic edifices using digital elevation models. Geomorphology 136: 114-131. https://doi.org/10.1016/j.geomorph.2011.06.001
- Grosse, P.; Ochi Ramacciotti, M.L.; Escalante Fochi, F.; Guzmán, S.; Orihashi, Y.; Sumino, H. 2020. Geomorphology, morphometry, spatial distribution and ages of mafic monogenetic volcanoes of the Peinado and Incahuasi fields, southernmost Central Volcanic Zone of the Andes. Journal of Volcanology and Geothermal Research 401: 106966. https://doi.org/10.1016/j.jvolgeores.2020.106966
- Haag, M.B.; Báez, W.A.; Sommer, C.A.; Arnosio, J.M.; Filipovich, R.E. 2019. Geomorphology and spatial distribution of monogenetic volcanoes in the southern Puna Plateau (NW Argentina). Geomorphology 342: 196-209. https://doi.org/10.1016/j.geomorph. 2019.06.008

- Heit, B.; Bianchi, M.; Yuana, X.; Kay, S.M.; Sandvol, E.; Kumara, P.; Kind, R.; Alonso, R.N.; Brown, L.D.; Comte, D. 2014. Structure of the crust and the lithosphere beneath the southern Puna plateau from teleseismic receiver functions. Earth and Planetary Science Letters 385: 1-11. https://doi.org/10.1016/j.epsl.2013.10.017
- Jordan, T.E.; Isacks, B.L.; Allmendinger, R.W.; Brewer, J.A.; Ramos, V.A.; Ando, C.J. 1983. Andean tectonics related to geometry of the subducted Nazca plate. Geological Society of America Bulletin 94: 341-361. http://dx.doi.org/10.1130/0016-7606(1983)94%3C34 1:ATRTGO%3E2.0.CO;2
- Kereszturi, G.; Németh, K. 2012. Monogenetic basaltic volcanoes: genetic classification, growth, geomorphology and degradation. *In* Updates in Volcanology-New Advances in understanding volcanic systems (Németh, K.; editor). IntechOpen: 3-88. https://doi.org/10.5772/51387
- Kshirsagar, P.; Siebe, C.; Guilbaud, M.N.; Salinas, S. 2016. Geological and environmental controls on the change of eruptive style (phreatomagmatic to Strombolianeffusive) of Late Pleistocene El Caracol tuff cone and its comparison with adjacent volcanoes around the Zacapu basin (Michoacán, México). Journal of Volcanology and Geothermal Research 318: 114-133. https://doi.org/10.1016/j.jvolgeores.2016.03.015
- Maisonnave, E.B. 2016. Petrología y evolución del volcanismo Neógeno y Cuaternario al sur de 24° LS y al Oeste de 67°30' O, Puna, Provincia de Salta, Argentina. Ph.D. Thesis (Unpublished). Universidad de Buenos Aires: 327 p.
- Maisonnave, E.B.; Poma, S. 2016. Caracterización petrológica y nuevas edades de los Basaltos de Chuculaqui, Puna Austral, Provincia de Salta. Revista de la Asociación Geológica Argentina 73 (4): 582-587.
- Maro, G.; Caffe, P.J.; Báez, W. 2017. Volcanismo monogenético máfico cenozoico de la Puna. *In* Ciencias de la Tierra y Recursos Naturales del NOA (Muruaga, C.M.; Grosse, P.; editors). *In* Congreso Geológico Argentino, No. 20, Relatorio: 548-577. San Miguel de Tucumán.
- Munk, L.A.; Boutt, D.F.; Moran, B.J.; McKnight, S.V.; Jenckes, J. 2021. Hydrogeologic and geochemical distinctions in freshwater-brine systems of an Andean salar. Geochemistry, Geophysics, Geosystems 22 (3): 1-20. https://doi.org/10.1029/2020GC009345
- Murcia, H.; Németh, K. 2020. Effusive monogenetic volcanism. *In* Updates in Volcanology-Transdisciplinary Nature of Volcano Science (Németh, K.; editor). IntechOpen: 1-15. https://doi.org/10.5772/intechopen.94387

- Németh, K.; Kereszturi, G. 2015. Monogenetic volcanism: personal views and discussion. International Journal of Earth Sciences 104: 2131-2146. https://doi.org/10.1007/ s00531-015-1243-6
- Németh, K.; Kósik, S. 2020. Review of explosive hydrovolcanism. Geosciences 10 (2): 44. https://doi. org/10.3390/geosciences10020044
- Pedrazzi, D.; Cerda, D.; Geyer, A.; Martí, J.; Aulinas, M.; Planagumà, L. 2022. Stratigraphy and eruptive history of the complex Puig de La Banya del Boc monogenetic volcano, Garrotxa Volcanic Field. Journal of Volcanology and Geothermal Research 423: 107460. https://doi.org/10.1016/j.jvolgeores.2021.107460
- Petrinovic, I.A.; Grosse, P.; Guzmán, S.; Caffe, P. 2017. Evolución del volcanismo Cenozoico en la Puna Argentina. *In* Ciencias de la Tierra y Recursos Naturales del NOA (Muruaga, C.M.; Grosse, P.; editors). Relatorio del Congreso Geológico Argentino, No. 20: 469-483. San Miguel de Tucumán.
- Planagumà, L.; Bolós, X.; Martí, J. 2023. Hydrogeologic and magmatic controls on phreatomagmatism at the La Garrotxa monogenetic volcanic field (NE of Iberian Peninsula). Journal of Volcanology and Geothermal Research 441: 107894. https://doi.org/10.1016/j.jvolgeores.2023.107894
- Riller, U.; Oncken, O. 2003. Growth of the Central Andean Plateau by tectonic segmentation is controlled by the gradient in crustal shortening. The Journal of Geology 111 (3): 367-384. https://doi.org/10.1086/373974
- Risse, A.; Trumbull, R.; Coira, B.; Kay, S.; van den Bogaard, P. 2008. ⁴⁰Ar/³⁹Ar geochronology of basaltic volcanism in the back-arc region of the southern Puna plateau, Argentina. Journal of South American Earth Sciences 26 (1): 1-15. https://doi.org/10.1016/j.jsames.2008.03.002
- Rosen, M.R. 1994. The importance of groundwater in playas: A review of playa classifications and the sedimentology and hydrology of playas. Geological Society of America Special Papers 289: 1-18. https://doi.org/10.1130/SPE289-p1
- Salfity, J.A.; Monaldi, C.R.; Marquillas, R.A.; Álvarez, L. 2005. Región de la Puna. *In* Frontera exploratoria de la Argentina (Chebli, G.A.; Cortiñas, J.; Lagarreta, L.; Spalletti, L.A.; Vallejo E.; editors). Simposio del Congreso de Exploración y Desarrollo de Hidrocarburos, No. 6: 77-95. Mar del Plata.
- Schoenbohm, L.M.; Carrapa, B. 2015. Miocene-Pliocene shortening, extension and mafic magmatism support small scale lithospheric foundering in the central Andes, NW Argentina. *In* Geodynamics of

- a Cordilleran Orogenic System: The Central Andes of Argentina and Northern Chile (DeCelles, P.G.; Ducea, M.N.; Carrapa, B.; Kapp, P.A.; editors). Geological Society of America Memoirs 212: 167-180. https://doi.org/10.1130/2015.1212(09)
- Schofield, N.; Alsop, I.; Warren, J.; Underhill, J.R.; Lehné, R.; Beer, W.; Lukas, V. 2014. Mobilizing salt: Magma-salt interactions. Geology 42 (7): 599-602. https://doi.org/10.1130/G35406.1
- Siebert, L.; Simkin, T.; Kimberly, P. 2010. Volcanoes of the World, 3rd edition. University of California Press: 551 p. Berkeley
- Smith, I.E.M.; Németh, K. 2017. Source to surface model of monogenetic volcanism: a critical review. *In* Monogenetic Volcanism (Németh, K.; Carrasco-Núñez, G.; Aranda-Gómez, J.J.; Smith, I.E.M.; editors). Geological Society of London, Special Publications 446: 1-28. https://doi.org/10.1144/SP446.14
- Stern, C.R. 2004. Active Andean volcanism: its geologic and tectonic setting. Revista Geológica de Chile 31 (2): 161-206. http://dx.doi.org/10.4067/S0716-02082004000200001
- Trumbull, R.; Riller, U.; Oncken, O.; Scheuber, E.;
 Munier, K.; Hongn, F. 2006. The time-space distribution of Cenozoic arc volcanism in the Central Andes: a new data compilation and some tectonic considerations. *In* The Andes-Active Subduction Orogeny (Oncken, O.; Chong, G.; Franz, G.; Giese, P.; Götze, H-J.; Ramos, V.; Strecker, M.; Wigger, P.; Editors). Frontiers in Earth Science, Series 1, Springer-Verlag: 29-43.
 Berlin. https://doi.org/10.1007/978-3-540-48684-8
- Turner, J.C.M.; Méndez, V. 1979. Puna. *In* Geología Regional Argentina (Turner, J.C.M.; editor). Academia Nacional de Ciencias: 13-56. Córdoba.
- Ureta, G.; Németh, K.; Aguilera, F.; Vilches, M.; Aguilera, M.;
 Torres, I.; Sepúlveda, J-P.; Scheinost, A.; González, R.
 2020. An overview of the mafic and felsic monogenetic
 Neogene to Quaternary volcanism in the Central
 Andes, Northern Chile (18-28°Lat.S). *In* Updates in
 Volcanology-Transdisciplinary Nature of Volcano
 Science (Németh, K.; editor). IntechOpen: 1-28.
 https://doi.org/10.5772/intechopen.93959
- Valentine, G.A.; Graettinger, A.H.; Sonder, I. 2014. Explosion depths for phreatomagmatic eruptions. Geophysical Research Letters 41 (9): 3045-3051. https://doi.org/10.1002/2014GL060096
- Valentine, G.A.; Connor, C.B. 2015. Basaltic volcanic fields. *In* The Encyclopedia of Volcanoes, 2nd edition

- (Sigurdsson, H.; Houghton, B.; McNutt, S.; Rymer, H.; Stix, J.; editors). Academic Press: 423-439. San Diego. https://doi.org/10.1016/B978-0-12-385938-9.00023-7
- Valentine, G.A.; Fierstein, J.; White, J.D. 2022. Pyroclastic deposits of Ubehebe Crater, Death Valley, California, USA: Ballistics, pyroclastic surges, and dry granular flows. Geosphere 18 (6): 1926-1957. https://doi.org/10.1130/GES02526.1
- Vandervoort, D.S.; Jordan, T.E.; Zeitler, P.K.; Alonso, R.N. 1995. Chronology of internal drainage development and uplift, southern Puna plateau, Argentine central Andes. Geology 23 (2): 145-148. https://doi. org/10.1130/0091-7613(1995)023%3C0145:COIDD A%3E2.3.CO;2
- Vespermann, D.; Schmincke, H.U. 2000. Scoria cones and tuff rings. *In* Encyclopedia of Volcanoes (Sigurdsson, H.; Houghton, B.F.; McNutt, S.R.; Rymer, H.; Stix, J.; editors). Academic Press: 683-694. San Diego.
- Viramonte, J.G.; Galliski, M.A.; Araña Saavedra, V.; Aparicio, A.; García Cucho, L.; Martín Escorza, C. 1984. El finivulcanismo básico de la depresión de Arizaro, provincia de Salta. *In* Congreso Geológico Argentino, No. 9, Actas 3: 234-251. Bariloche.
- Wadell, H.A. 1933. Sphericity and roundness of rock particles. The Journal of Geology 41 (3): 310-331. https://www.jstor.org/stable/30058841
- Warren, J.K. 2006. Evaporites: Sediments, resources and hydrocarbons. Springer: 1036 p. Berlin.
- White, J.D.L. 1996. Impure coolants and interaction dynamics of phreatomagmatic eruptions. Journal of Volcanology and Geothermal Research 74 (3-4): 155-170. https://doi.org/10.1016/S0377-0273(96)00061-3
- White, J.D.L.; Houghton, B.F. 2006. Primary volcaniclastic rocks. Geology 34 (8): 677-680. https://doi.org/10.1130/G22346.1
- White, J.D.L.; Ross, P.S. 2011. Maar-diatreme volcanoes: a review. Journal of Volcanology and Geothermal Research 201 (1-4): 1-29. https://doi.org/10.1016/j.jvolgeores.2011.01.010
- White, J.D.L.; Valentine, G.A. 2016. Magmatic versus phreatomagmatic fragmentation: Absence of evidence is not evidence of absence. Geosphere 12 (5): 1478-1488. https://doi.org/10.1130/GES01337.1
- Zappettini, E.O.; Blasco, G. 2001. Hoja Geológica 2569-II Socompa, Provincia de Salta. Instituto de Geología y Recursos Minerales, Servicio Geológico Minero Argentino, Boletín 260: 62 p. Buenos Aires.